Basin Research (2002) **14,** 105–127

Interactions between onshore bedrock-channel incision and nearshore wave-base erosion forced by eustasy and tectonics

N.P. Snyder,* K.X. Whipple,* G.E. Tucker† and D.J. Merritts‡

**Department of Earth, Atmospheric and Planetary Sciences, Massachusetts Institute of Technology, Cambridge, Massachusetts 02139-4307, USA*
† School of Geography and the Environment, University of Oxford, Oxford OX1 3TB, UK
‡Department of Geosciences, Franklin and Marshall College, Lancaster, Pennsylvania 17604-3003, USA

ABSTRACT

We explore the response of bedrock streams to eustatic and tectonically induced fluctuations in base level. A numerical model coupling onshore fluvial erosion with offshore wave-base erosion is developed. The results of a series of simulations for simple transgressions with constant rate of sea-level change (SLR) show that response depends on the relative rates of rock uplift (U) and wave-base erosion (ε_w). Simple regression runs highlight the importance of nearshore bathymetry. Shoreline position during sea-level fall is set by the relative rate of base-level fall (U-SLR) and ε_w, and is constant horizontally when these two quantities are equal. The results of models forced by a realistic Late Quaternary sea-level curve are presented. These runs show that a stable shoreline position cannot be obtained if offshore uplift rates exceed ε_w. Only in the presence of a relatively stable shoreline position, fluvial profiles can begin to approximate a steady-state condition, with U balanced by fluvial erosion rate (ε_f). In the presence of a rapid offshore decrease in rock-uplift rate (U), short (~5 km) fluvial channels respond to significant changes in rock-uplift rate in just a few eustatic cycles. The results of the model are compared to real stream-profile data from the Mendocino triple junction region of northern California. The late Holocene sea-level stillstand response exhibited by the simulated channels is similar to the low-gradient mouths seen in the California streams.

INTRODUCTION

The response of fluvial systems to eustatic fluctuations is a classic problem in sedimentology (e.g. Wheeler, 1964; Middleton, 1973; Vail *et al.*, 1977; Pitman, 1978; Christie-Blick & Driscoll, 1995). In general, the previous analyses focused on transgressions, when sea level rises, shifting the locus of deposition onshore; and regressions, when sea level drops, incising onshore and pushing deposition farther offshore. The geomorphic literature has also given some attention to the development of topography and bathymetry in response to eustatic sea-level change. A number of workers have studied and modelled longitudinal profile development of large rivers in coastal alluvial settings (e.g. Schumm, 1993; Talling, 1998; Antoine *et al.*, 2000; Tebbens *et al.*, 2000). The creation of fluvial terraces has been used as a template for discussing responses to tectonics, climate and eustasy (e.g. Merritts *et al.*, 1994; Pazzaglia *et al.*, 1998; Veldkamp & Van Dijke, 2000). Numerous workers have studied the development of marine terraces with respect to sea level and tectonics (e.g. Bloom *et al.*, 1974; Chappell, 1974; Merritts & Bull, 1989; Cinque *et al.*, 1995). The concentrated energy expenditure of waves breaking on shorelines drives landward erosion of a wave-cut notch, creating a platform, if relative sea level remains constant for a sufficiently long time. On uplifting coastlines, prominent marine platforms are developed during periods of rising sea level. If the platform is raised above the surf zone (through increased surface uplift or sea-level fall or both), then it becomes a marine terrace. Recently, Anderson *et al.* (1999) used a simple model for wave-base erosion in order to investigate the cutting and uplift of marine terraces on a tectonically active coastline. Here we build on and compliment these research themes by exploring the response of coastal bedrock streams to variations in sea level and associated marine erosion—we study the channels rather than the interfluves and terraces developed around them. Our approach is to link a model

Correspondence: N.P. Snyder, USGS Pacific Science Center, 1156 High Street, Santa Cruz, California 95064, USA. E-mail: nsnyder@usgs.gov

© 2002 Blackwell Science Ltd

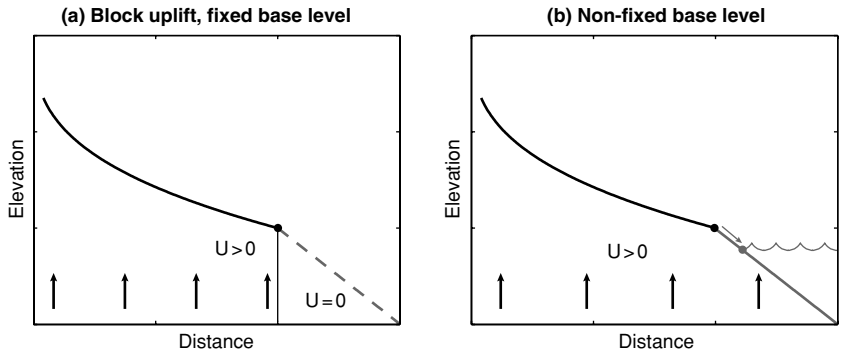

Fig. 1. Block uplift and base-level demonstration. (a) An example of a typical fluvial channel model. A concave-up stream longitudinal profile (solid line) is uplifted vertically at a constant rate, relative to a fixed base-level outlet point (marked by the black dot). Physically, this base level must mark a significant discontinuity in deformation, for instance a fault. To the right of the dot, the rock-uplift rate (U) drops as a step function to zero. This part of the profile (dashed line) is unimportant to models with this boundary condition. (b) Similar to (a), but here the entire profile uplifts at the same rate. In this case, fluvial base level (black dot) simply represents the change from subaerial (black line) to subaqueous conditions (gray line). If this base level drops (i.e. regression, grey dot), then the fluvial system will respond according to the gradient of the newly emergent channel (between the black dot and the gray dot).

for onshore, fluvial bedrock incision (e.g. Howard & Kerby, 1983; Stock & Montgomery, 1999; Snyder *et al.*, 2000) with the Anderson model for offshore erosion, for investigating the response of this coupled system to transgressions, regressions and Late Quaternary sea-level history. The goal is to gain first-order insight into the response of bedrock-floored streams actively incising coastal mountain belts to tectonically and eustatically driven base-level change.

Most recent modelling studies of fluvial response to uplift have treated the case of uplift relative to a fixed base level (Fig. 1a) (e.g. Whipple & Tucker, 1999; Snyder *et al.*, 2000; Tucker & Whipple, 2002). Put another way, these models fix the model lower boundary condition (stream outlet point) at a static elevation. This situation may be acceptable for some specialized tectonic settings, such as uplift of the footwall of a normal fault relative to the hanging wall, or uplift on a high-angle fault relative to a static water level. However, in the case where the fluvial base level migrates in space and time owing to eustasy, uplift and erosion, as with streams on uplifting coastlines, this boundary condition is clearly an oversimplification. Here we present a model with a more realistic treatment for the base-level condition (Fig. 1b). Other workers (e.g. Willet *et al.*, 2001) have emphasized the role of horizontal advection of topography, as in the case of uplift on the hanging wall of a thrust ramp. This response is also important for the development of fluvial topography, but for simplicity we do not include it in our modelling efforts. However, a horizontal component of rock motion could be easily incorporated into the model presented here (e.g. Kirby & Whipple, 2001).

In order to begin our investigation of bedrock-channel response to uplift and eustasy, we present a simple thought experiment. Figure 2 shows a series of hypothetical situations for onshore and offshore topography, similar to the cases suggested by Summerfield (1985, 1991) and Schumm (1993). The onshore is represented by a concave-up longitudinal stream profile, whereas the offshore is a linear ramp with various gradients. In this scenario, fluvial base level (sea level) is changed from the initial condition (triangle) to the final condition (circle), in the absence of uplift or erosion (except in Fig. 2d). The first two panels represent regressions across an offshore that is flatter than the onshore channel (Fig. 2a) and steeper than the onshore (Fig. 2b). In the first case, we expect a decrease in the ability of the stream to erode and/or transport sediment, so the emergent platform will likely inhibit erosion and induce deposition of a prograding wedge of sediment. In the second case, the newly emergent section of stream is steep, and so rapid channel incision will occur, perhaps generating a knickpoint that propagates upstream. The third and fourth panels show the results of a transgression. In Fig. 2(c), sea level inundates the lower part of the channel, with little effect on the profile, aside from shortening the stream. This situation is, of course, unrealistic because in this thought experiment we are ignoring onshore and offshore erosion. Figure 2(d) is the same as Fig. 2(c), except that significant wave-base erosion occurs during the transgression, driving a knickpoint up the channel mouth. The difference between the two panels (Fig. 2c and d) highlights the importance of understanding the interplay of changing base level and erosion patterns. It is this interplay that we will examine in this paper.

The central question of the modelling exercises presented here is: what is the response of an erosional fluvial system to the combined forcings of tectonic rock uplift, eustatic sea-level fluctuations and offshore wave-base erosion? We approach this question by starting with the simplest cases of transgressions and regressions (constant rate of sea-level rise or fall) on uplifting coastal rivers. In these experiments, we want to know when the model predicts enhanced onshore erosion (represented by a knickpoint propagating onshore, i.e. Fig. 2b and d), or a

© 2002 Blackwell Science Ltd,

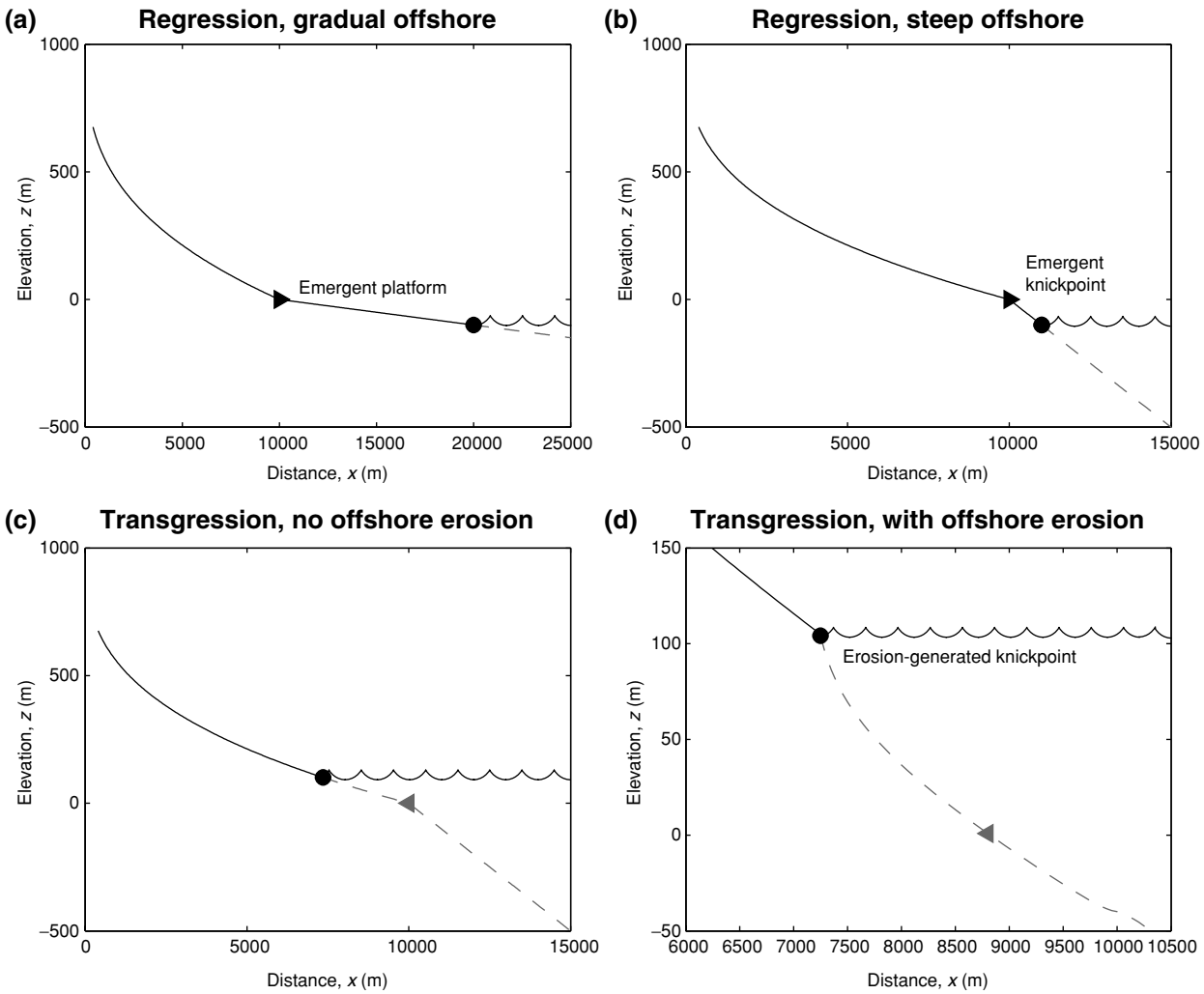

Fig. 2. Cartoon examples of model regressions and transgressions, without uplift or erosion (in a–c). In each panel, the initial location of sea level is marked by the triangle (pointing in the direction of motion of the coastline) and the final location is marked by the dot and scalloped line. To the left of the triangle is a concave-up stream longitudinal profile; to the right is a bathymetric ramp of constant gradient. Note that the scale is different in each figure. (a) Regression over a gradual offshore. The emergent stream segment is relatively flat, and will therefore likely be a zone of deposition. (b) Regression over a steep offshore. The emergent channel is a knickpoint, responding with high incision rates. (c) Transgression without offshore erosion. The location of the fluvial base level moves up the channel without any significant response. (d) Transgression with offshore erosion. If offshore, wave-base erosion rates are high, then the seabed at the transgressing shoreline will be steep, pushing a knickpoint onshore.

flat platform (Fig. 2a), or no response of the channel (Fig. 2c). Once we establish how the model parameters set these responses to a simple sea-level forcing function, we present the second set of experiments by using a realistic Late Quaternary sea-level curve. Because present-day topography and bathymetry represent the integrated effects of the history of forcings, we investigate stream response to the sea-level fluctuations associated with the last few glacial–interglacial cycles. Here the questions turn to the model predictions with respect to the morphology of Late Quaternary tectonic coasts. What channel-mouth morphology is expected at the end of a major transgression? Under what range of parameter space do we expect emergence of a marine terrace and seaward advancement of the shoreline? How do offshore conditions influence the onshore morphology? What does the model predict about steady-state erosion conditions and the development of fluvial relief? In the final part of this paper, model predictions are compared to a well-studied suite of streams in northern California (Merritts & Vincent, 1989; Snyder *et al*., 2000; Snyder *et al*., 2002a). We begin with a brief discussion of the model onshore and offshore erosion laws and a synopsis of the model execution.

MODEL FORMULATION

We are concerned with the response of a coupled system—with erosion of bedrock by onshore and offshore processes—to tectonic and eustatic forcing. The modelling presented here is meant to apply to uplifting, rocky coastlines, with onshore erosional channels and offshore wave-cut platforms. The model addresses only channel and

nearshore longitudinal profile response—not the evolution of interfluves and headlands—as studied by Anderson *et al.* (1999). We make the simplifying assumption that both onshore and offshore processes are detachment-limited; in other words, that lowering rates are set by the ability to break off pieces of intact bedrock. In such systems, the sediment created by bedrock detachment is transported rapidly away (to the far offshore), with only minor, temporary storage in floodplains, fans, terraces and beaches. Some of this storage may have important geomorphic implications, but for simplicity the work presented here contains only qualitative inferences about the role of sediment transport and deposition. Adding sediment flux to model transport-limited fluvial conditions (e.g. Willgoose *et al.*, 1991; Sklar & Dietrich, 1998; Veldkamp & Van Dijke, 1998; Tucker *et al.*, 2001; Whipple & Tucker, 2002) remains an important next step to extend the applicability of the model to a wider range of settings and to understand key details of Holocene coastal morphology. Here we are limited essentially to the case of bedrock-floored streams cutting narrow canyons as they cross emergent marine terraces, not sediment-controlled factors such as construction of alluvial fans at channel mouths or the backfilling of bedrock canyons with alluvium that may occur during sea-level rises. Our initial goal is to capture the first-order response of detachment-limited systems. This model is most likely applicable to small drainage basins (drainage area, $A < 50\,\mathrm{km}^2$) undergoing rapid rock-uplift rates ($U > 0.001\,\mathrm{m\,year}^{-1}$).

Onshore fluvial incision

Incision of bedrock by rivers (ε_f, defined as positive downward) is often modelled as a power-law function of basal shear stress or unit stream power, either of which can be expressed as a function of channel gradient (S) and drainage area (A) (Howard & Kerby, 1983; Whipple & Tucker, 1999):

$$\varepsilon_f = KA^m S^n \tag{1}$$

where K is a dimensional coefficient dependent on a variety of factors (Stock & Montgomery, 1999; Whipple & Tucker, 1999), and m and n are exponents dependent on erosion process, channel width and discharge. We use the version of Eqn. (1) that applies to detachment-limited bedrock incision. Theoretical predictions for the value of n range from 2/3 to 5/3, but the best field estimates are typically from 2/3 to 1 (Howard & Kerby, 1983; Stock & Montgomery, 1999; Whipple *et al.*, 2000; Kirby & Whipple, 2001). The ratio of the exponents (m/n) is generally found to be between 0.4 and 0.6 (from theory and observation, e.g. Snyder *et al.*, 2000), though exceptions have been reported (Sklar & Dietrich, 1998). For simplicity, we use $m = 0.5$ and $n = 1$. The influence of the plausible range of m and n has been discussed elsewhere (Howard *et al.*, 1994; Whipple & Tucker, 1999; Snyder *et al.*, 2000; Tucker & Whipple, 2002), and here the emphasis is on the interaction between the onshore and the offshore. Though we have shown previously that this model is oversimplified in its omission of a realistic treatment of climate and a threshold shear stress to initiate incision (Snyder, 2001; Snyder *et al.*, 2002a,b), for the purposes of this study Eqn. (1) is sufficient, because it does capture the first-order form and tectonic response of channel longitudinal profiles with a minimum of free parameters (Snyder *et al.*, 2000).

In the case where channel incision (ε_f) balances rock-uplift rate (U, defined as positive upward, with a steady-state condition: $U = \varepsilon_f$), U can be substituted for ε_f in Eqn. (1), yielding a solution for steady-state slope (S_e):

$$S_e = \left(\frac{U}{K}\right)^{1/n} A^{-m/n} \tag{2}$$

This theoretical steady-state power-law relationship between S and A is similar in form to a commonly observed empirical relation:

$$S = k_s A^{-\theta} \tag{3}$$

where the coefficient k_s is the channel 'steepness index', and θ is the profile 'concavity index'. For comparison of empirical parameters from slope–area regressions to theoretical model inputs, we define a new variable, k_{si} equal to $(U/K)^{1/n}$, the theoretical steady-state channel steepness for a given set of parameters. Equations (2) and (3) are equivalent if and only if (i) $U = \varepsilon_f$, and (ii) U, K, m and n do not vary downstream, as discussed by Snyder *et al.* (2000). In reality, these criteria are only approximately met in most field settings, because they implicitly require that the channel is uplifted vertically on a block relative to a fixed base level, and that none of the factors that go into K (e.g. climate, lithology and possibly sediment flux relative to carrying capacity) varies downstream. Previously we have studied the role of controls on K, including discharge (and associated climate), lithology, channel width and sediment flux (Snyder, 2001; Snyder *et al.*, 2002a,b). These factors are intentionally not considered here, because we would like to isolate the effect that a fluctuating base level has on channel form and response.

Offshore wave-base erosion

We are concerned with development of nearshore bathymetry over 10–100 kyr timescales in uplifting, tectonically active coastlines, where shelf sediment deposition and storage are minimal. Compared to the fluvial system, this situation has received relatively little attention in the geomorphic literature, though cliffed, rocky coastlines are common throughout the world (Sunamura, 1992). The most comprehensive treatment of the problem is the numerical modelling work by Anderson *et al.* (1999), which dealt with the two-dimensional evolution of marine terraces. Faced with a similar problem, here we use the Anderson model to describe the erosion of the shelf. The basic postulate of the model is that seabed erosion rate (ε_w, defined positive downward) is a linear function of the rate

© 2002 Blackwell Science Ltd,

of energy dissipation (dE/dt), which can be expressed as an exponential function of water depth:

$$\varepsilon_w = \beta(dE/dt) = \beta(dE/dt)_o \exp(-4h/h_{wb}) = \beta' \exp(-4h/h_{wb}) \quad (4)$$

where $(dE/dt)_o$ is the energy dissipation rate in very shallow water, h is the water depth, h_{wb} is the depth where dE/dt is essentially zero (the wave base) and β is a dimensional coefficient that relates the rate of dissipation of wave energy to erosion rate. Because we have no constraints on the value of either $(dE/dt)_o$ or β, we simply use β' as an adjustable parameter that encompasses both $(dE/dt)_o$ and β ($\beta' = \beta(dE/dt)_o$). For the problem of offshore bedrock platform erosion, the effective wave base (h_{wb}) is also essentially unknown, and this parameter sets the width of the shelf affected by erosion.

Anderson *et al*. (1999) were concerned with the development of coastal cliffs, which form the inner edges of marine terraces. They modelled sea-cliff retreat by integrating the wave energy dissipated on the shelf and by assuming that the rest of the energy is expended in horizontal cliff retreat. In this way, they simulated the effect of increased or decreased wave dissipation across a wide or narrow shelf, respectively. Though this model may be appropriate for interfluvial areas where cliff erosion is driven by undercutting by waves and subsequent mass wasting, it is not appropriate for the mouths of channels where cliffs are not present and erosion is driven by a combination of wave and fluvial processes. We do not include the cliff-retreat component of the Anderson model in our efforts, because it would simply act to impart an additional lowering on the model node just upstream of sea level. This simplification has one obvious advantage and one disadvantage. Equation (4) indicates that wave-base erosion rate (ε_w) is a maximum when the water depth (h) is zero—consistent with the idea that breaking waves are the most powerful in driving erosion. This means that the maximum and most important value of ε_w is described by only one unknown parameter (β'), making the application to modelling quite simple. However, because dissipation rate (dE/dt) is purely a function of h, and not the change in amount of incoming wave energy owing to interaction with shelf bathymetry (dE/dx), the width and slope of the shelf have no effect on ε_w, making this model a clear oversimplification—we expect that erosion as a result of waves breaking on the shoreline should be less for a wide, flat shelf than for a narrow, steep shelf (Adams *et al*., 2000). This limitation means that the model cannot predict the long-term development of nearshore bathymetry. Therefore, we limit application to single transgressions and regressions, and a few glacial–interglacial cycles. Lacking a more sophisticated model for wave-base erosion (which would necessarily involve more unknown parameters), we proceed with this simple approach, which is sufficient to capture the first-order interaction between onshore and offshore erosion processes over short timescales (< 1 Myr).

MODEL SETUP: ALL CASES

We now outline the application of model, including initial profile conditions, uplift-rate boundary conditions and the coupling of the two erosion models. We explore the response of uplifting coastlines, in general, to simple transgressions and regressions in the first modelling exercise, and in the second part we take the specific example of the last few glacial–interglacial cycles (120–782 kyr). In the latter experiments, the resulting landforms are compared to the topography and bathymetry of a series of previously studied channels in northern California (Merritts & Vincent, 1989; Snyder *et al*., 2000; Snyder, 2001; Snyder *et al*., 2002a,b). For both cases, we use some parameter values derived from the California field area, but we emphasize that the results are generally applicable to uplifting coastlines and that the conclusions reached are independent of the particular parameter values used.

Initial conditions

The model profiles consist of evenly spaced (50 m) horizontal nodes (distance downstream, x), with elevations (z) decreasing from the top of the fluvial system (about 300–400 m downstream from the divide; Snyder *et al*., 2000) to the end of the offshore profile. For the onshore, fluvial part of the profile, the initial condition is simply a model steady-state channel, for block uplift relative to a fixed base level, generated using an integrated form of Eqn. (2), and an empirical power-law relationship (parameterized from data in the northern California study area, similar to that of Hack, 1973) between drainage area (A) and distance downstream (x) (Fig. 3). Various profiles are generated for both low (0.5 mm year^{-1}) and high (4 mm year^{-1}) uplift-rate conditions by using average parameters from Snyder *et al*. (2000) (Table 1). For the offshore part of the profile, a linear ramp of constant gradient ($S_{ramp} = 0.01$–0.1) was used—with the range of S_{ramp} chosen on the basis of the northern California nearshore bathymetry—in order to yield cases where the offshore is flatter or steeper than the onshore (Fig. 3). Only the relative gradients are important—not the absolute values. The onshore drainage area function is assumed to extend offshore, but applies only when subaerially exposed—a simplification not expected to affect model results significantly.

Uplift-rate boundary conditions

As mentioned above, the profiles are subjected to rock-uplift rates of 0.5 and 4 mm year^{-1} (Fig. 3). This is the range measured in the northern California study area (Merritts & Bull, 1989), and it is representative of tectonically active coastlines, in general. The model has uniform uplift rate for the entire onshore portion of the initial profile, and part of the offshore portion, in some model configurations. At some distance offshore, the uplift rate makes a rapid, linear decrease (over 5 km in x) to zero at the

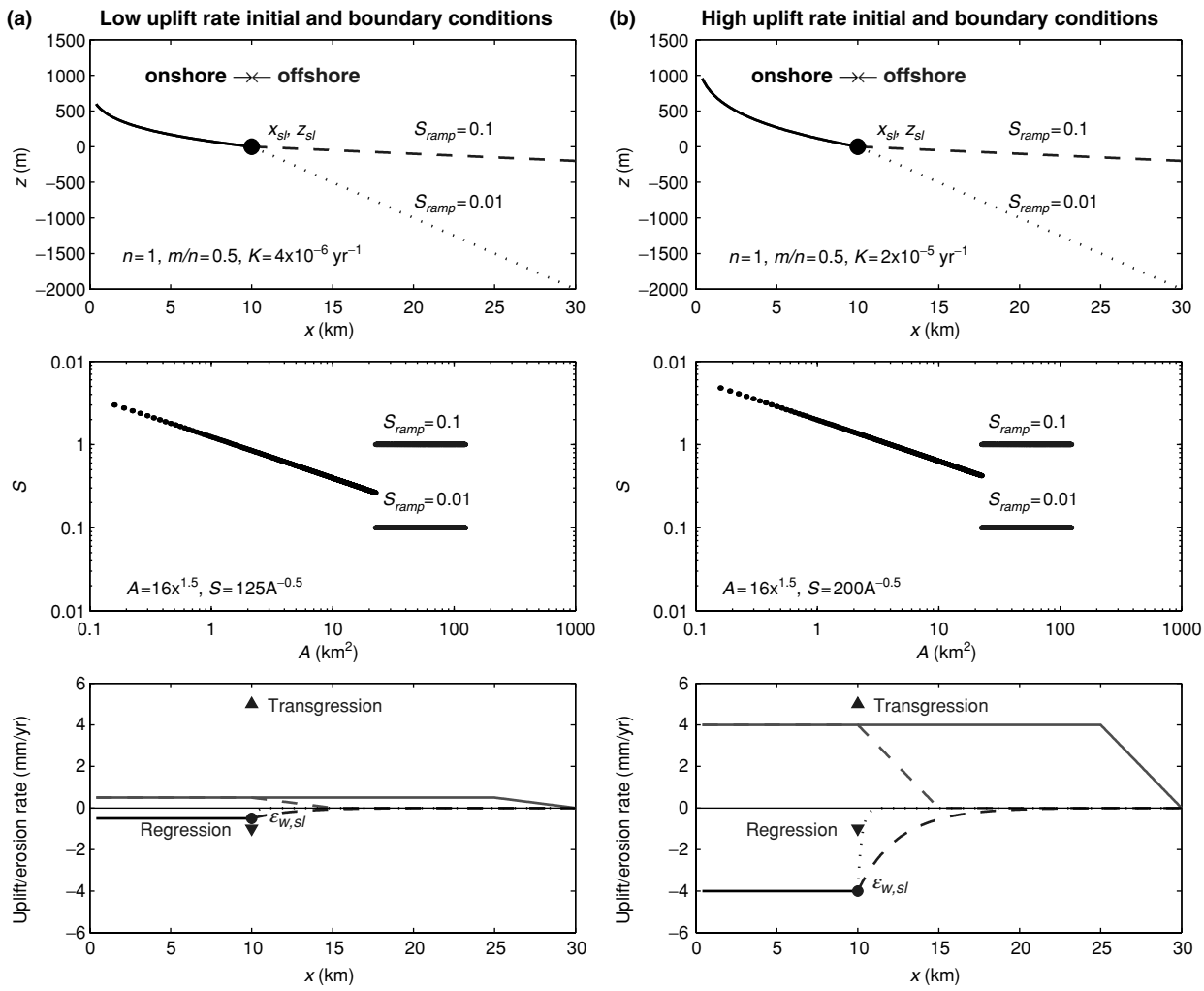

Fig. 3. Model initial and boundary conditions. Top panels are initial longitudinal profiles: a concave-up stream channel (solid line), adjusted to the uplift rate for a fixed base–level boundary condition (i.e. Figure 1a) and two offshore conditions, gradual ($S_{ramp} = 0.01$, dashed line) and steep ($S_{ramp} = 0.1$, dotted line). The black dot marks the initial shoreline position. Parameter values for the onshore stream profiles are shown in the lower left corner. Middle panels are log-space slope (S) vs. drainage area (A) plots, for the longitudinal profiles in the top panels. Bottom panels compare the four rates relevant to stream response. Gray, positive lines are rock-uplift rates (U), which are constant for the length of initial stream profile, and drop rapidly (over 5 km) to zero at some position in the offshore. In the constant-uplift-rate boundary condition (solid gray line) the rate is constant until a point far enough offshore that it will not be part of the model erosion domain during regressions, so that the offshore boundary does not influence the model results. In the uplift-rate gradient boundary condition (dashed gray line), the steep gradient in U begins at the initial shoreline. Triangles represent the rates of sea-level rise (transgression) and fall (regression) used for the simple model runs. Black lines below zero represent initial erosion rates, plotted as negative values for clarity. Onshore fluvial incision rate (ε_f, from Eqn. (2), solid line) is set in magnitude to equal U. Offshore wave-base erosion rate (ε_w, from Eqn. (4), dashed line for $S_{ramp} = 0.1$, dotted line for $S_{ramp} = 0.01$) is varied in the model runs. The maximum value occurs at sea level ($\varepsilon_{w,sl}$). (a) The left panels are for low-uplift conditions ($U = 0.0005$ m year^{-1}). (b) The right panels are for high-uplift conditions ($U = 0.004$ m year^{-1}).

seaward (right) boundary (Fig. 3, bottom panels). This gradient is arbitrarily chosen, and it is simply meant to represent a decrease in uplift rate distributed over a narrow zone, such as might occur at a fault zone. We used two different positions for the boundary of the uplifting block: (i) far enough offshore so that the erosive part of the model does not interact with the uplift ramp during the entire model run (typically at least 15 km from the initial shoreline)—termed the constant uplift-rate boundary condition—and (ii) at the initial shoreline—termed the uplift-rate gradient boundary condition (Fig. 3, bottom panels). In the first boundary condition, the uplift-rate drop is unimportant to the model, whereas in the second boundary condition the spatially variable uplift rates are directly important to the system response. These two cases allow us to isolate the role of the uplift-rate boundary conditions.

© 2002 Blackwell Science Ltd,

Table 1. Model parameters.

General	
U	rock-uplift rate, positive upward (m year^{-1})
SLR	rate of sea-level rise or fall (m year^{-1})
A	drainage area (m^2)
S	topographic gradient (m/m)
t	model time (year)
z	elevation, relative to sea level at $t = 0$ (m)
z_{sl}	elevation of sea level at time t (m)
x	horizontal distance downstream from divide (m)
x_{sl}	horizontal position of the sea-level node (m)
S_{ramp}	gradient of the model offshore ramp
h	water depth (m)
Onshore fluvial incision (Eqns (1) and (2))	
ε_f	vertical fluvial incision rate, positive downward (m year^{-1})
m	drainage-area exponent m = 0.5
n	slope exponent $n = 1$
K	coefficient of fluvial incision (m^{1-2m} year^{-1})
$K = 4 \times 10^{-6}$ year^{-1} for $U = 0.0005$ m year^{-1} and $m = 0.5$	
$K = 2 \times 10^{-5}$ year^{-1} for $U = 0.004$ m year^{-1} and $m = 0.5$	
(values chosen to match basin relief in Snyder *et al.*, 2000)	
S_e	theoretical steady-state channel gradient
k_{si}	theoretical steady-state channel steepness index (m$^{2m/n}$, from $k_{si} = (U/K)^{1/n}$)
$k_{si} = 125$ m for $K = 4 \times 10^{-6}$ year^{-1}	
$k_{si} = 200$ m for $K = 2 \times 10^{-5}$ year^{-1}	
m/n	theoretical steady-state channel concavity index $m/n = 0.5$
Empirical fluvial parameters	
k_s	channel steepness index (m$^{2\theta}$, from Eqn. (3))
θ	channel concavity index
k_{s2}	channel steepness index, from regression with $\theta = 0.5$
k_a	coefficient (m$^{2-\alpha}$, from $A = k_a x^{\alpha}$)
$k_a = 15.6$ m$^{0.46}$ (for 10 km model streams, from Juan Creek; Snyder *et al.* 2000)	
$k_a = 4.72$ m$^{0.28}$ (for 5 km model streams, from Kinsey Creek; Snyder *et al.* 2000)	
α	Exponent $\alpha = 1.54$ (for 10 km model streams, from Juan Creek; Snyder *et al.* 2000)
$\alpha = 1.72$ (for 5 km model streams, from Kinsey Creek; Snyder *et al.* 2000)	
Offshore wave-base erosion (Eqn. (4))	
ε_w	vertical wave-base erosion rate, positive downward (m year^{-1})
$\varepsilon_{w,sl}$	vertical wave-base erosion rate at sea level ($h = 0$) (m year^{-1})
E	wave energy (J)
dE/dt	wave energy dissipation rate (J year^{-1})
dE/dx	horizontal spatial derivative of wave energy (J m^{-1})
β	wave-energy coefficient (m J^{-1})
$(dE/dt)_o$	wave-energy dissipation rate in very shallow water (J year^{-1})
β'	adjustable parameter, $\beta' = \beta(dE/dt)_o$ (m year^{-1})
h_{wb}	depth of wave base (m)
$h_{wb} = 100$ m for all model runs presented here	

Coupling of erosion laws

The model response depends fundamentally on the relative magnitudes of four rates: rock uplift (U), onshore incision (ε_f, initially set equal to U), sea-level change (SLR) and offshore erosion (ε_w, set by β'), and we focus on these values in the presentation of model results. The bottom panels in Fig. 3 show the initial values of each of these rates, for the various initial profile conditions. Once the model is running, ε_f and ε_w vary based on the topography and bathymetry and apply to a domain of nodes defined by the location of the shoreline (x_{sl}). In practice, each model time step involves the following sequence of four steps:

A new sea level (z_{sl}) is calculated, based on an input function. The model node with elevation closest to this value is assigned to be the sea-level node (x_{sl}).

Fluvial erosion rate (ε_f) is calculated based on Eqn. (1) for all nodes landward of x_{sl}, by using the downstream slope.

Wave-base erosion rate (ε_w) is calculated based on Eqn. (4) for all nodes from x_{sl} to the offshore boundary.

All nodes are uplifted and eroded an amount equal to the sum of U and the applicable erosion rate (ε_f or ε_w) multiplied by the time step (dt).

MODEL RESULTS AND INTERPRETATION 1: GENERAL CASES

Approach

For the general cases we used simple, constant-rate, sea-level functions that roughly approximate the last glacial regression (100 m fall in 100 kyr) and transgression (100 m rise in 20 kyr). We explored a large range of parameter space, systematically varying the offshore erosion rate coefficient (β'), wave base (h_{wb}), uplift rate (U), uplift boundary condition and offshore bathymetry (S_{ramp}). We use two uplift-rate cases, with corresponding initial onshore erosion rates (ε_f set equal to U), and two sea-level cases, as well as two S_{ramp} values and two positions of the U boundary condition (Fig. 3, bottom panels). Once the model begins to run, the onshore erosion rate at any given node varies freely as channel gradient (S) changes. For simplicity, we used only one value of wave base ($h_{wb} = 100$ m) for all of the model results shown here, because h_{wb} affects only the width of the shelf affected by wave-base erosion, and therefore it plays a secondary role in channel response. Because ε_w reaches a maximum at sea level ($h = 0$, $\varepsilon_{w,sl}$), that sets the response, in the discussion of the results we focus on this value (not β'). We have done model runs varying $\varepsilon_{w,sl}$ from zero to values greater than the relative rate of base-level change (U-SLR). We present a sampling of plots that are representative of the full parameter space —chosen to highlight key aspects of channel response to eustatic forcing. The central question with each run is how the morphology of the previously steady-state river mouth is affected by the combined forcings of eustasy and uplift—that is, generation of a knickpoint or flat platform. We include some interpretation of the results of the transgression and regression cases in their respective subsections, and a brief discussion of the overall implications for the general modelling in the last part of this section.

Transgressions

The initial profile conditions for the transgression cases are simply a steady-state stream onshore ($\varepsilon_f = U$) and a steep ramp ($S_{ramp} = 0.1$) offshore (Fig. 4). Because the rate of sea-level rise ($SLR = 5$ mm year^{-1}) is faster than uplift rate, the offshore conditions are unimportant. The entire onshore profile is uplifted at a constant rate.

The response of channels to such rapid transgression is straightforward. Because SLR is always greater than U, the streams shorten as the ocean inundates the channel. The response of the mouth and nearshore is set by the relative difference between U and $\varepsilon_{w,sl}$. If uplift rate equals or is on the same order as offshore erosion rate ($U \approx \varepsilon_{w,sl}$), then there is no effect on the onshore part of the profile, and the nearshore flattens slightly as the inundated channel approaches h_{wb} (Fig. 4a). If uplift rate greatly exceeds offshore erosion rate ($U > \varepsilon_{w,sl}$), then the mouth of the channel flattens (as it moves onshore), as does the nearshore (Fig. 4b). Finally, if wave-base erosion rate exceeds uplift rate ($U < \varepsilon_{w,sl}$), then a knickpoint at the channel mouth, created by wave-base erosion, is driven upstream with the rising sea level, and a flat platform is created in the nearshore (Fig. 4c and d).

Regressions

Modelling channel response to regressions is more complicated than the transgression case, because the offshore profile and uplift boundary conditions become important. In order to explore the range of possibilities, we use two different offshore ramp gradients (S_{ramp}) and two different uplift boundary conditions. In the regression case, the rate of sea-level decline ($SLR = -1$ mm year^{-1}) is in the opposite direction from the uplift rate (U), subjecting the channel to an increased rate of relative base-level change (U-SLR). For this reason, the channel grows seaward at a maximum rate (for small ε_w) of (U-SLR)/S_{ramp}. Here, we consider the regression modelling in three parts: (i) gradual S_{ramp}, (ii) steep S_{ramp} (both with the constant uplift-rate boundary condition outside of model domain affected by erosion) and (iii) a steep S_{ramp} with the uplift-rate gradient boundary condition (Fig. 3). Note that as a gradual S_{ramp} and a proximal boundary to the uplifting block are mutually inconsistent (because the position of the channel mouth would regress out of the model domain), only the steep S_{ramp} condition is considered in this case.

Figure 5 shows four model results for regression over a gradual ramp ($S_{ramp} = 0.01$), with the uplift-rate boundary condition seaward of the domain affected by erosion. This value of S_{ramp} is less than the slope of the channel mouth. In the case where the wave-base erosion rate is less than the rate of base-level fall ($\varepsilon_{w,sl} < U$-SLR), a wide, gradual platform emerges, as the position of the channel mouth (x_{sl}) regresses over the gradual ramp (Fig. 5a, b, and d). The emergent, low-gradient channel is not only flatter than the steady-state initial condition, but it also has a different concavity index (θ), because of the seaward motion of x_{sl}. Below, we investigate this further. If offshore erosion balances the relative position of sea level ($\varepsilon_{w,sl} = U$-SLR), then x_{sl} remains fixed, lowering at rate SLR, and the channel mouth steepens as a knickpoint is developed (Fig. 5c). This occurs because wave-base erosion (ε_w) removes the uplifting seabed instead of regressing along the ramp. The high ε_w also causes the offshore to be bladed off at an extremely low slope. Of course, if ε_w is even faster than U-SLR ($\varepsilon_{w,sl} > U$-SLR), then x_{sl} actually transgresses and drives a knickpoint inland (a case not shown in Fig. 5).

Figure 6 illustrates the same model runs as Fig. 5, but with a value of S_{ramp} greater than the slope of the channel mouth (for both low-uplift and high-uplift cases). The key difference is seen in Fig. 6(a), where the low-uplift-rate channel mouth gets steeper as it regresses onto the ramp.

© 2002 Blackwell Science Ltd,

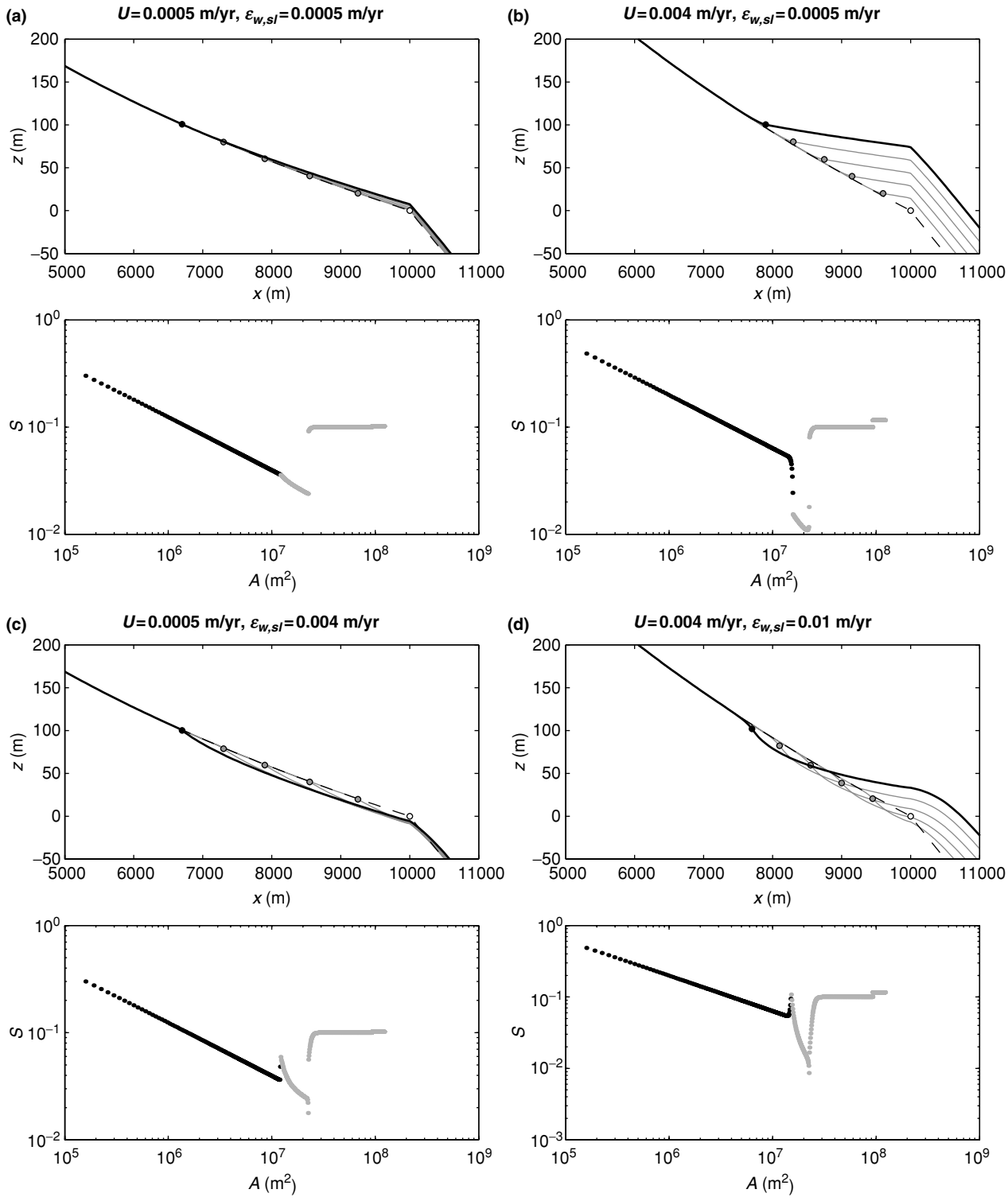

Fig. 4. Model runs for simple transgressions ($SLR = 0.005$ m year^{-1} for 20 kyr). Top panels show detailed views of the longitudinal profiles, with initial conditions (dashed lines), four evenly spaced (in model time) intermediate conditions (gray lines) and final condition (black lines). Location of sea level for each profile is marked by the circles (open for initial, gray for intermediate, black for final). Bottom panels are slope (S) vs. drainage area (A) plots for the final profiles. Onshore points are shown in black; offshore points are shown in gray. Note that the drainage area values used for the offshore points are only applicable if they become onshore points, and are only used here for clarity in plotting. See Table 1 for parameter values used in all model runs. (a) Low-uplift rate, low wave-base erosion rate case. (b) High-uplift rate, low wave-base erosion rate case. (c) Low-uplift rate, high wave-base erosion rate case. (d) High-uplift rate, high wave-base erosion rate case.

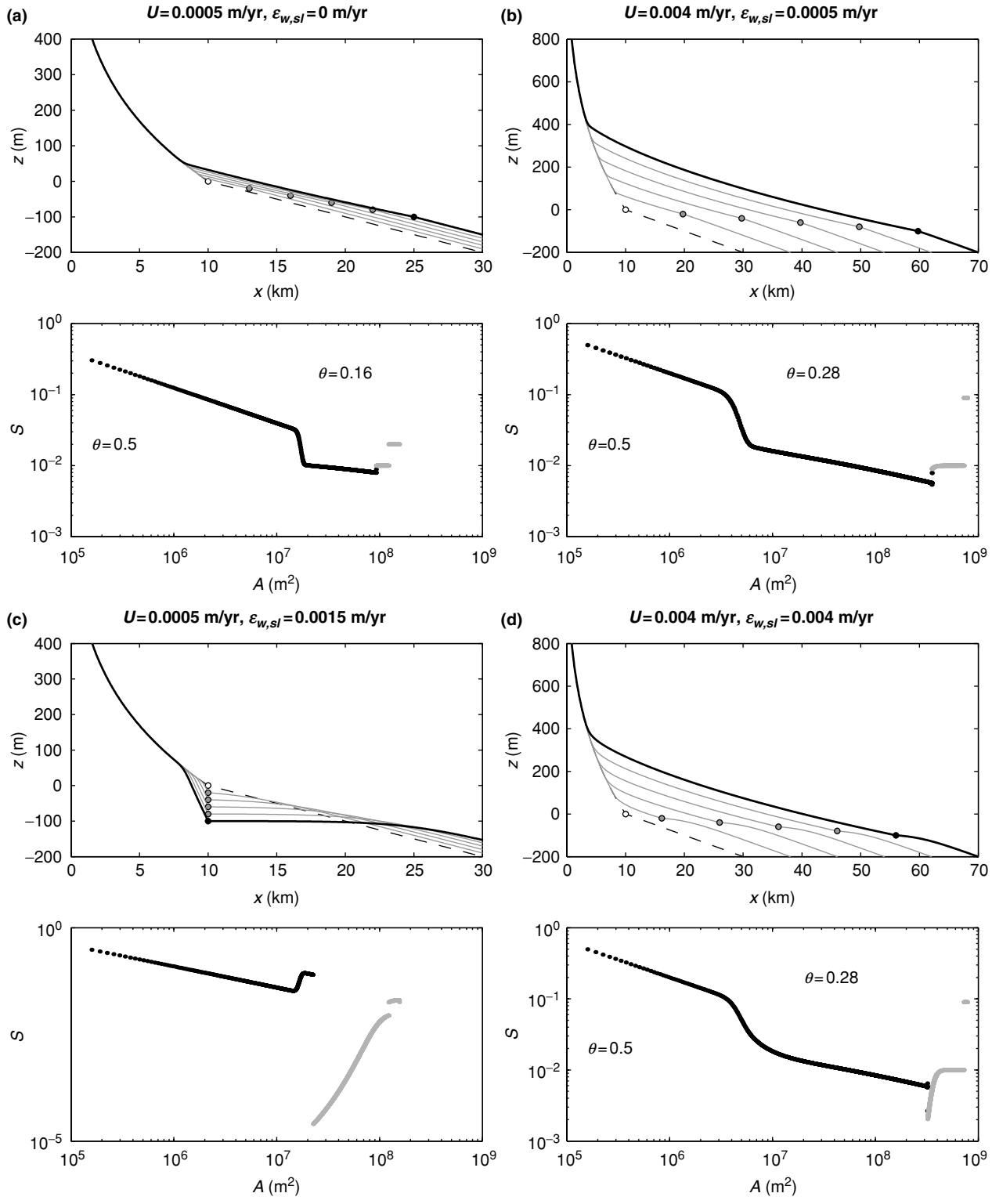

Fig. 5. Model runs for simple regressions ($SLR = -0.001$ m year^{-1} for 100 kyr), with a gradual offshore ramp ($S_{ramp} = 0.01$), and constant uplift rate throughout the modelled erosion domain. Note that the scale is different in the top panels. See Fig. 4 for description. (a) Low-uplift rate, no wave-base erosion case. (b) High-uplift rate, low wave-base erosion case. (c) Low-uplift rate case, with wave-base erosion set to balance relative rate of base-level fall ($\varepsilon_{w,sl} = U$-SLR). (d) High-uplift rate, moderate-high wave-base erosion rate case.

Conversely, Fig. 6(b,d) shows that for high U, the channel mouth is actually less steep—a gradual platform is created, in spite of the initially steep offshore ramp. Figure 6(c), where the x_{sl} is fixed, is little different from Fig. 5(c).

The new channel profile segments created during a regression exhibit a lower concavity index (θ) than the fixed base-level steady-state initial channel (Figs 5 and 6), because the base level is both dropping and extending

© 2002 Blackwell Science Ltd,

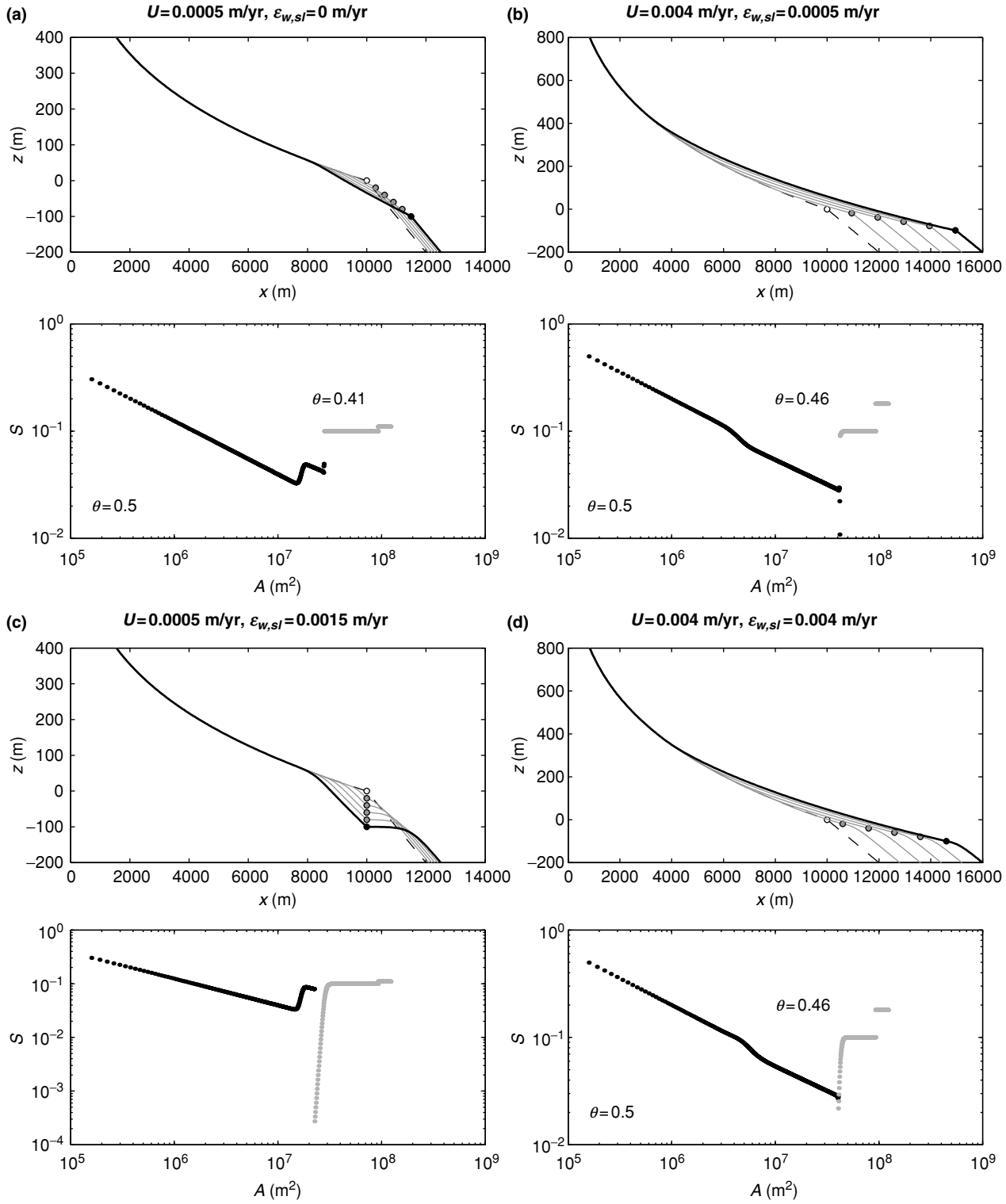

Fig. 6. Model runs for simple regressions ($SLR = -0.001$ m year^{-1} for 100 kyr), with a steep offshore ramp ($S_{ramp} = 0.1$), and constant uplift rate throughout the modelled erosion domain. All cases are the same as Fig. 5. See Fig. 4 for general description.

seaward. This new concavity is set by S_{ramp}, U, SLR and $\varepsilon_{w,sl}$, and exists because the relationship between onshore distance and drainage area ($A = k_a x^{\alpha}$) continues into the newly emergent channel (Fig. 3). The channel does exhibit a steady-state form (slope unchanging with time), but it is not strictly speaking a 'steady-state channel' because the mouth is constantly migrating seaward, extending its length, and the whole channel is experiencing net uplift at a uniform rate. If the model is allowed to run indefinitely, with an infinitely long ramp, the channel eventually achieves this new steady form from mouth to divide.

When uplifting a ramp, instead of uplift relative to a fixed base level, the maximum onshore slope at the outlet (and therefore maximum ε_f) is set by the gradient of the offshore ramp, provided the wave-base erosion rate is low (Figs 5a,b and 6a,b). In the high-uplift cases ($U = 4\,\text{mm year}^{-1}$), this situation causes the newly created stream to be less steep than the initial condition for all but the steepest ramps ($S_{ramp} >> 0.5$). In the low-uplift cases ($U = 0.5\,\text{mm year}^{-1}$), the mouth is steeper than the initial condition for S_{ramp} greater than about 0.05. This observation highlights the importance of understanding the controls on the development of bathymetry to adequately predict channel response to eustatic regressions. A proper erosion law for offshore bedrock platforms is needed (including the effects of sediment deposition, shelf width, distribution of storms, cutting of offshore canyons, etc.) to be able to model long-term (~1 Myr) evolution of nearshore bathymetry.

When the shoreline position (x_{sl}) regresses through variable rock-uplift rates (uplift-rate gradient boundary condition), results are much more complicated, particularly in the high-uplift cases because of the steep gradient in U immediately offshore from the initial condition (Fig. 7). In these cases, U linearly decreases over 5 km in the offshore from a maximum of the onshore uplift rate at the initial location of x_{sl} (Fig. 3). The steep bathymetric ramp is used ($S_{ramp} = 0.1$, as in Fig. 6). Figure 7(d) shows that as x_{sl} regresses to the zone experiencing lower uplift rates, the rate of horizontal seaward migration slows and eventually halts at the point where $\varepsilon_{w,sl}$ equals U-SLR, continuously lowering the outlet at rate SLR, as in the examples shown in Figs 5(c) and 6(c). This yields significant changes in the width (narrower) and slope (steeper) of the emergent channel segment that is created during regression in high-U conditions (compare with Fig. 6d). The low-U cases are not particularly different from the cases where the uplift rate is constant throughout the entire erosive part of the system, because the U gradient is less dramatic. However, the long-term evolution of the profiles would be quite different, because the location of x_{sl} would eventually regress to the point where $\varepsilon_{w,sl} = U$-SLR (as seen in Fig. 7d). Comparisons among runs with the uplift-rate gradient over shorter and longer horizontal distances (not shown) indicate that the presence of an offshore uplift-rate gradient is much more important to the model results than the magnitude of the gradient. These uplift-rate gradient boundary condition examples simply serve to show that uplift-rate boundary condition is critical in setting the topographic response of streams to eustatic sea-level changes and rock uplift.

In summary, the results of the general modelling of regressions indicate that the initial bathymetry is critical in setting the response of the onshore stream channel. Within a range of plausible values of the offshore slope ($S_{ramp} = 0.01$–0.1), the $U = 0.5\,\text{mm year}^{-1}$ cases exhibit steeper emergent channel segments for greater values of S_{ramp}. The $U = 4\,\text{mm year}^{-1}$ cases persistently exhibit flat emergent platforms, unless the regression occurs across a significant uplift-rate gradient boundary. These results are modified by high wave-base erosion rates ($\varepsilon_{w,sl} > U$-SLR). In all regression cases, channel response is quite different from that predicted by the simple case of uplift relative to a fixed base level—that is, $S_{ramp} = 8$.

Interpretation of general model results

The simple models of transgressions and regressions presented above show that the development of nearshore bathymetry is critical to setting the response of uplifting rivers to eustatic sea-level fluctuations. Bathymetry has direct implications during regressions, as we have shown. During transgressions, bathymetry has only an indirect influence, presumably modulating wave-base erosion rates, though this effect is not treated here. However, the simple cases presented so far capture only the influence of a single transgression or regression, starting with a known, simple initial condition. The situation becomes more complicated when a realistic sea-level curve is used in order to drive the model, as we do in the following section. In order to highlight this point, consider the transgression case (Fig. 4). Though the bathymetry is not important to stream profile during the sea-level rise, as soon as SLR is less than U (for low ε_w), the nearshore platform will begin to emerge, and the channel response to this relative regression will depend critically on the offshore profile. If this emergent platform is flat (e.g. Fig. 4b), then deposition will likely occur at the channel mouth, because the slope of the river would be insufficient to transport the sediment load—a factor that is not included in this model. Conversely, a knickpoint–flat platform pair may emerge, and this may have a more complicated response (e.g. Fig. 4d). In any case, this response will be set by the offshore topography developed during the transgression, which is set by wave-base erosion—a process that lacks a sophisticated geomorphic model at present. In the late Holocene (past ~6 kyr), global sea level is in a post-transgression stillstand situation as described above, making this scenario directly relevant to the study of modern river profiles. In the next section, we run the model forced by a realistic Late Quaternary sea-level curve and compare the onshore and offshore topography predicted by the model to that of the Mendocino triple junction area of northern California.

MODEL RESULTS AND INTERPRETATION 2: LATE QUATERNARY SEA-LEVEL FUNCTION

Approach

We now move beyond a constant rate of sea-level change in order to explore the response of the model to realistic eustatic fluctuations. In this second set of experiments, the model is forced by a realistic Late Quaternary sea-level curve. The deep-sea oxygen isotope record is a reasonable proxy for glacial ice volume and therefore sea level (e.g. Chappell *et al.*, 1996). We use the stacked, normalized

© 2002 Blackwell Science Ltd,

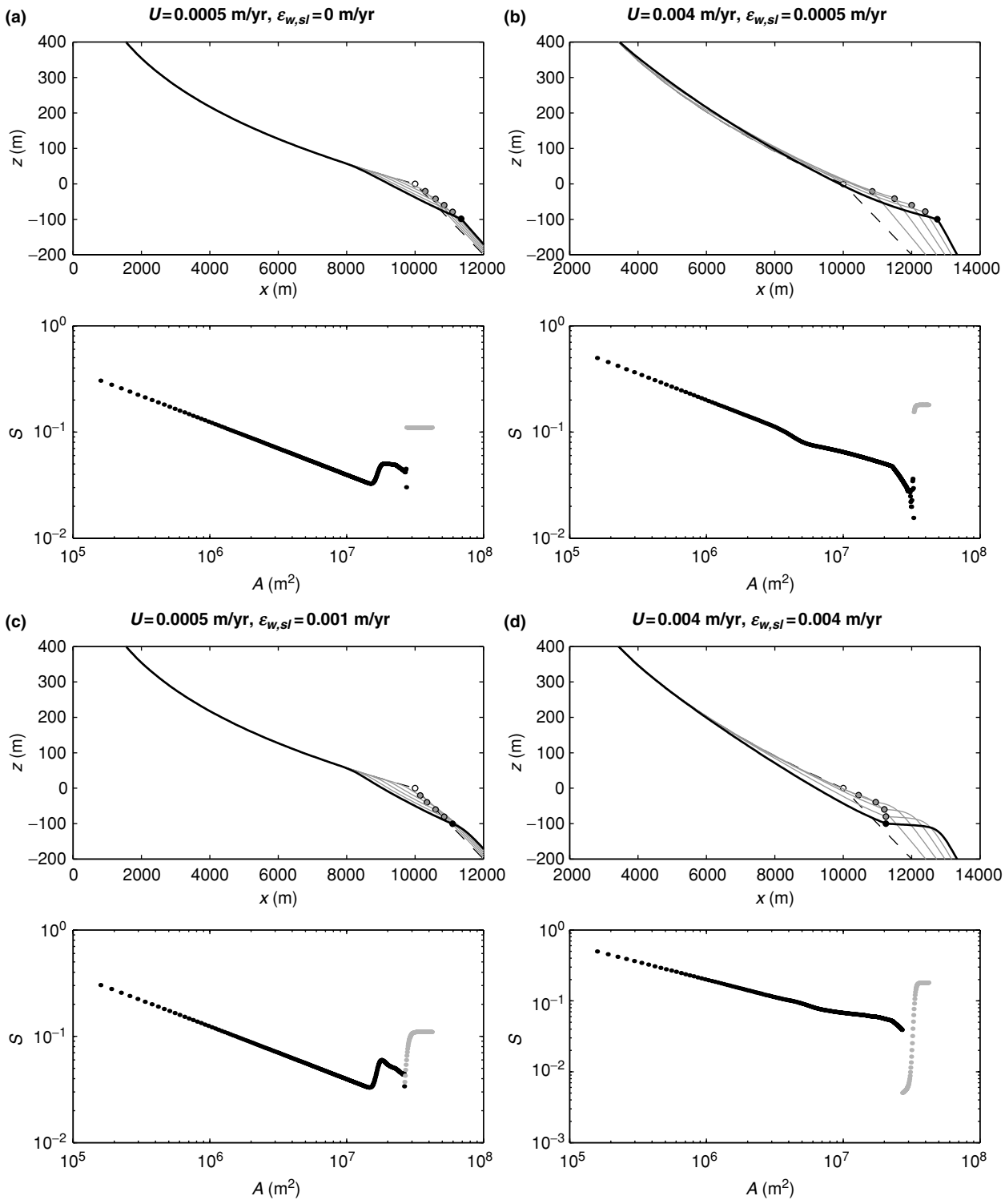

Fig. 7. Model runs for simple regressions ($SLR = -0.001$ m year^{-1} for 100 kyr), with a steep offshore ramp ($S_{ramp} = 0.1$), and the uplift-rate gradient boundary condition (steep drop at the location of the initial shoreline). (a) Low-uplift rate, no wave-base erosion case. (b) High-uplift rate, low wave-base erosion case. (c) Low-uplift rate case, moderate wave-base erosion case. (d) High-uplift rate, moderate-high wave-base erosion rate case.

SPECMAP δ^{18}O record of Imbrie *et al.* (1984), transformed via a second-order polynomial to produce a reasonable, continuous approximation of Quaternary sea level (Fig. 8), as shown by Anderson *et al.* (1999). This record begins at a negative δ^{18}O excursion (highstand) at 782 ka. Our purpose with this modelling is not to attempt to reproduce exactly present-day topography, but to investigate model response to a realistic sea-level history. Therefore, though the transformation from δ^{18}O is imperfect and approximate, as is the timing of the

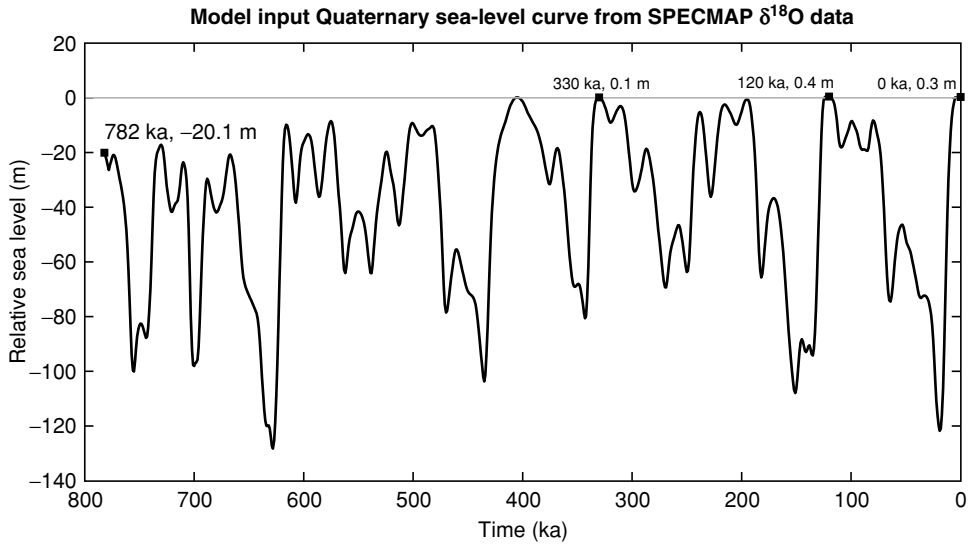

Fig. 8. Approximate Late Quaternary sea-level curve used as model input. Original data is the Imbrie *et al.* (1984) stacked, normalized SPECMAP δ^{18}O curve. This is transformed to sea level via an empirical polynomial (relative sea level = -32.841-($33.747\delta^{18}$O)-($8.5605(\delta^{18}O)^2$)) (Anderson *et al.*, 1999). Various highstand times and sea levels, used as model initial times, are indicated by labelled boxes.

δ^{18}O record, the sea-level curve shown in Fig. 8 is certainly adequate for our purpose, in as much as it is a reasonable representation of the rate and magnitude of eustatic sea-level fluctuations over the Late Quaternary (Anderson *et al.*, 1999).

For this experiment, we investigated both the response to a single glacial–interglacial cycle and the model prediction for how fluvial topography evolves over time. Therefore, for each set of initial conditions, the model was run from the previous interglacial highstand (120 ka) to the present highstand, and for three or more highstands (330–782 ka) to the present (Fig. 8). These longer runs de-emphasize the importance of initial conditions. All of the runs start at a highstand and end at the present.

For the initial stream longitudinal profile, we used a 5 km channel, developed in the same way as the first experiment (for parameters see Table 1). This shorter channel has the advantage that the model profile responds rapidly, reaching a constant form in less time than a channel 10 km long. This length also allows direct comparison with the northern California streams discussed below (Snyder *et al.*, 2000). As before, we used two values of rock-uplift rate (U) and two positions for the edge of the uplifting block. We also investigated the response to a change from a low-uplift rate scenario to a high-uplift rate scenario. In order to further de-emphasize the importance of initial conditions, the model runs presented here use offshore ramp gradients (S_{ramp}) chosen to match the outlet slopes for the various uplift conditions ($S_{ramp} = 0.05$ for $U = 0.0005\,\mathrm{m\,year^{-1}}$; $S_{ramp} = 0.1$ for $U = 0.004\,\mathrm{m\,year^{-1}}$). For simplicity, we also do not vary offshore erosion rates ($\varepsilon_w = 0.0005\,\mathrm{m\,year^{-1}}$) and wave base ($h_{wb} = 100\,\mathrm{m}$). We have already investigated how all of these parameters influence the response, and we discuss these results both in the previous sections and below.

The second set of experiments has two interrelated purposes, with associated questions. As in the first experiment, we investigate how sea-level forcing affects the channel mouth. We want to know (i) whether we expect knickpoints or flat platforms and (ii) whether the coastline is advancing or retreating through time. In the section entitled 'Discussion' the model results are compared to present-day coastal morphology in northern California.

The second purpose of this suite of experiments is to analyze the stream longitudinal profiles as a whole, by using models run for several glacial–interglacial cycles. In a previous study (Snyder *et al.*, 2000), we used regressions of data on channel gradient (S) vs. drainage area (A; Eqn. (3)) in order to estimate model parameters (Eqn. (2)). This analysis was based on the hypothesis that the channels were adjusted to block uplift relative to a fixed base level (Fig. 1). Here we can test the range of parameter space where the steady-state hypothesis is valid for a variable base level. This is performed by comparing empirical channel steepness index (k_s) and concavity index (θ) from S–A regressions of model profiles (Eqn. (3)) to input model parameters that correspond to steady-state steepness index ($(U/K)^{1/n} = k_{si}$) and concavity index (m/n, Eqns (1) and (2)). As we have previously discussed extensively (Snyder *et al.*, 2000), θ and k_s covary strongly, so for comparison purposes we calculate a value of steepness index (k_{s2}) for a fixed concavity index ($\theta = 0.5 = m/n$)—a technique directly analogous to the representative slope method of Sklar & Dietrich (1998). We also calculate slopes at 10 m contour intervals, both to minimize regression bias and to be consistent with our prior methodology (Snyder *et al.*, 2000). Finally, we further consider the question of steady state by investigating the response of channels to an acceleration in U, again comparing model profiles to those of our previous study (Snyder *et al.*, 2000).

© 2002 Blackwell Science Ltd,

Constant-uplift-rate boundary condition

Figure 9 illustrates the results of model runs for constant low and high rock-uplift rates, forced by 120 and 782 kyr of the Quaternary sea-level curves (Fig. 8). For a single glacial–interglacial cycle (120 kyr), the response depends largely on the initial offshore conditions. In the two cases shown (Fig. 9a and b), S_{ramp} is slightly steeper than the fluvial outlet slope. However, as seen in the previous regression experiments, the resulting emergent channel is, on average, slightly flatter than the original onshore channel gradient. For the low-uplift rate example ($U = 0.0005\,\mathrm{m\,year^{-1}}$, Fig. 9a), the response is quite subtle, with only a slight emergent platform forming. Because the rock-uplift rate equals the wave-base erosion rate at sea level ($U = \varepsilon_{w,sl}$) and the initial and final sea levels are the same in the model run, the shoreline position (x_{sl}, z_{sl}) has not changed. Moreover, the regression of onshore S–A data indicates that the overall profile has changed only a minor amount, with concavity index (slope of the regression line, θ) and steepness index (intercept of the regression line for a fixed value of θ, k_{s2}) equal to the initial values ($\theta = m/n = 0.5$; $k_s \approx k_{s2} \approx k_{si} = 125$), reflecting a small deviation from the steady-state condition. Conversely, in the high-uplift case ($U = 0.004\,\mathrm{m\,year^{-1}}$, Fig. 9b), the channel has several breaks in slope reflecting the complex history of sea-level rises and falls during the 120 kyr model period. The shoreline position has prograded seaward more than 3 km, lengthening the channel significantly. The channel mouth is an emergent flat platform, resulting from post-transgression uplift of the wave-cut platform during the late Holocene stillstand. The S–A data are not linear in log space, and the regression yields a high concavity index ($\theta = 0.56$), and low steepness index ($k_{s2} = 166$, compared to $k_{si} = 200$ for high-uplift conditions). In both cases, the upper parts of the channel do not deviate from the initial condition, indicating that the base-level perturbations have not yet affected the entire channel.

The 782 kyr model runs (Fig. 9c and d) have profiles that reflect the integrated effect of 7–8 glacial–interglacial cycles. In both cases, the channel has lengthened because of net uplift. Associated with the lengthening is a net decrease in channel gradient, as indicated by the low values of the observed steepness index (k_{s2}), when compared to those theoretically predicted for steady-state channels under with these parameter values ($k_{si} = 125$ for low-uplift channels; $k_{si} = 200$ for high-uplift channels). The perturbations propagate slowly through the low-uplift channel (Fig. 9c), and the uppermost part has yet to respond. In the high-uplift case (Fig. 9d), the entire channel has responded and is uplifting as the channel lengthens. Given even more time, the low-uplift channel will also begin to experience net uplift throughout. Because the channel is lengthening and overall relief (total elevation drop on the fluvial system) is increasing, a true steady state is impossible to attain in a situation with constant uplift rate throughout the model domain. However, as discussed previously, the channels are approaching a steady-state form, with an average concavity index (θ) near the model-input value (m/n), and a low steepness index (k_{s2}), as suggested in Fig. 9(d).

Uplift-rate gradient boundary condition

The results of four model runs with a steep gradient in uplift rate in the initial 5 km offshore are shown in Fig. 10. As before, the entire channels have not fully responded in one glacial–interglacial cycle (Fig. 10a and b). The effect on the low-uplift case is minor. The high-uplift case shows a set of migrating knickpoints and flats travelling up the channel, as well as the emergent wave-cut platform at the channel mouth.

In the 330 kyr model runs (Fig. 10c and d), both channels have responded to the fluctuating base level from their mouths to their divides. Experience with longer runs (up to 782 kyr) indicates that further changes to the profiles are extremely minor. Both channels have achieved a quasi-steady-state condition—the position of the channel does not change significantly in x or z over time. As in the simple regressions, the maximum seaward shoreline position is set by the place where the relative rate of base-level fall, set by the uplift rate (which is decreasing with increasing x) and the rate of sea-level fall, during regressions, balances the wave-base erosion rate ($\varepsilon_{w,sl}$). Because the magnitude and frequency of the regressions are reasonably constant, this position changes little once it is established. Therefore, the channels cease to lengthen significantly, even in high-uplift cases, and the profile achieves a quasi-steady-state position. In both cases, the S–A regressions indicate that the overall channel form (as indicated by θ and k_{s2}) is very similar to the input values ($m/n = 0.5$ and $k_{si} = 125$ or 200).

DISCUSSION

Steady-state channel profiles

A central goal of this modelling exercise is to establish what can be learnt from analysis of channel longitudinal profiles that experience complex base-level forcing. In order to use regressions of channel gradient against drainage area (S–A) for constraining model parameters (e.g. Snyder *et al.*, 2000), channels must be in a steady state, with fluvial erosion rates balancing rock-uplift rates ($\varepsilon_f = U$). The model results indicate that in the absence of an offshore decrease in uplift rates, steady state is impossible (Fig. 9). During the transient seaward advance of the shoreline (at a horizontal rate set by S_{ramp}), the channel should be less steep than the model prediction for a fixed base level, though concavity may be fairly close to the model prediction. The history of the advance should be recorded in an emergent flight of very wide (> 1 km per eustatic cycle) marine terraces (i.e. Figure 9d). In practice, such a situation (unrestricted advance of x_{sl} as a result of high-U offshore) may be short-lived (in geological terms), because the shoreline position will rapidly transgress until it

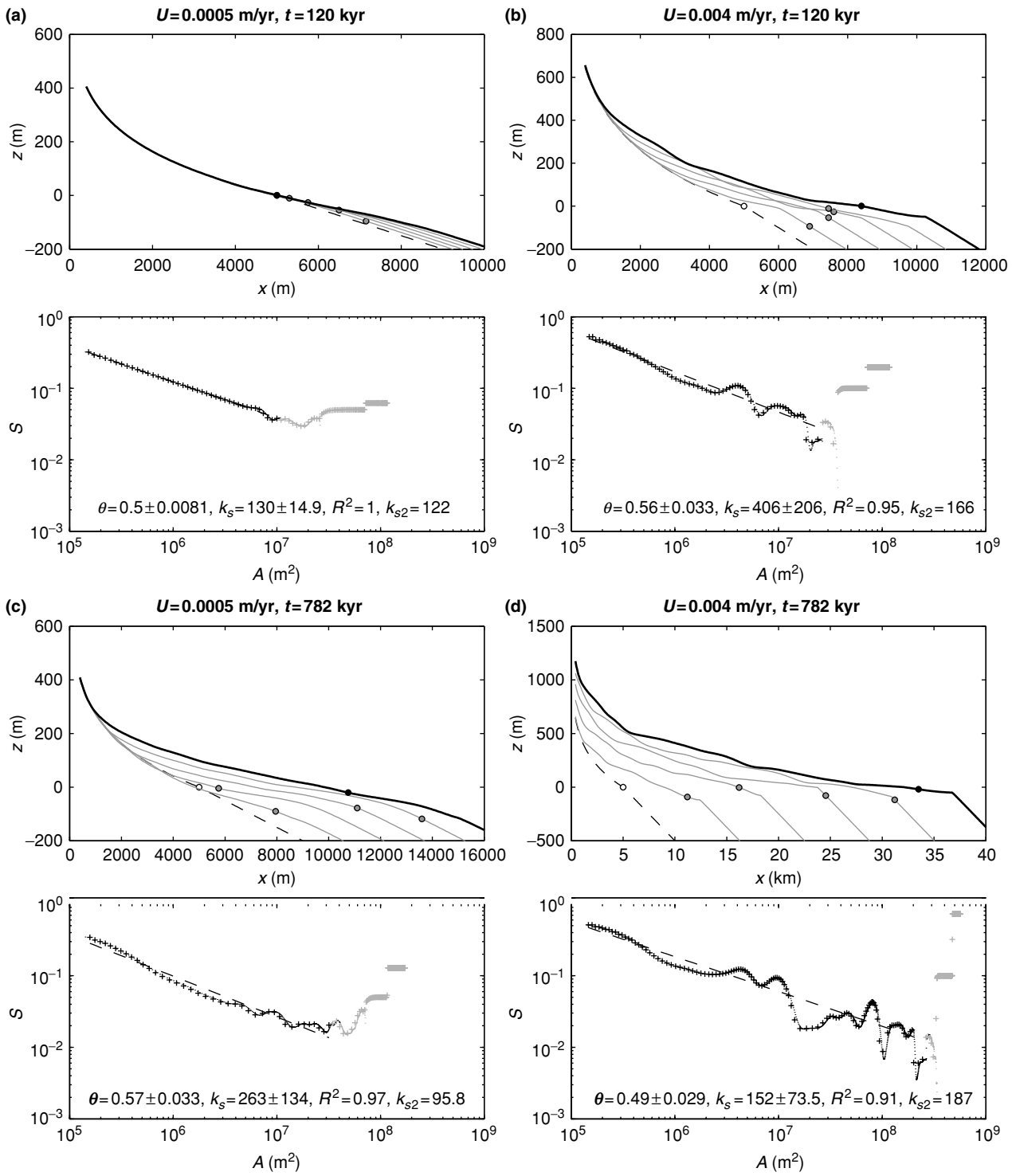

Fig. 9. Model results with Quaternary sea-level curve, and constant uplift rates throughout the erosive part of the offshore. General description of plots is the same as Fig. 4. Bottom panel (slope–area data) has crosses for channel gradient calculated on 10 m elevation contours, and small dots (often obscured) for slopes of individual data points. Dashed regression lines and regression values are calculated based on the contoured slope data. Offshore data points are shown in gray, and are not included in regressions. See text, Fig. 13 caption and Snyder *et al*. (2000) for further information about regression techniques. $\varepsilon_{w,sl} = 0.0005$ m year^{-1} or all model runs in Figs 9–11. (a) Single glacial–interglacial cycle (120 kyr), low-uplift rate. (b) Single glacial–interglacial cycle (120 kyr), high-uplift rate. (c) Multiple cycles (782 kyr), low-uplift rate. (d) Multiple cycles (782 kyr), high-uplift rate.

© 2002 Blackwell Science Ltd,

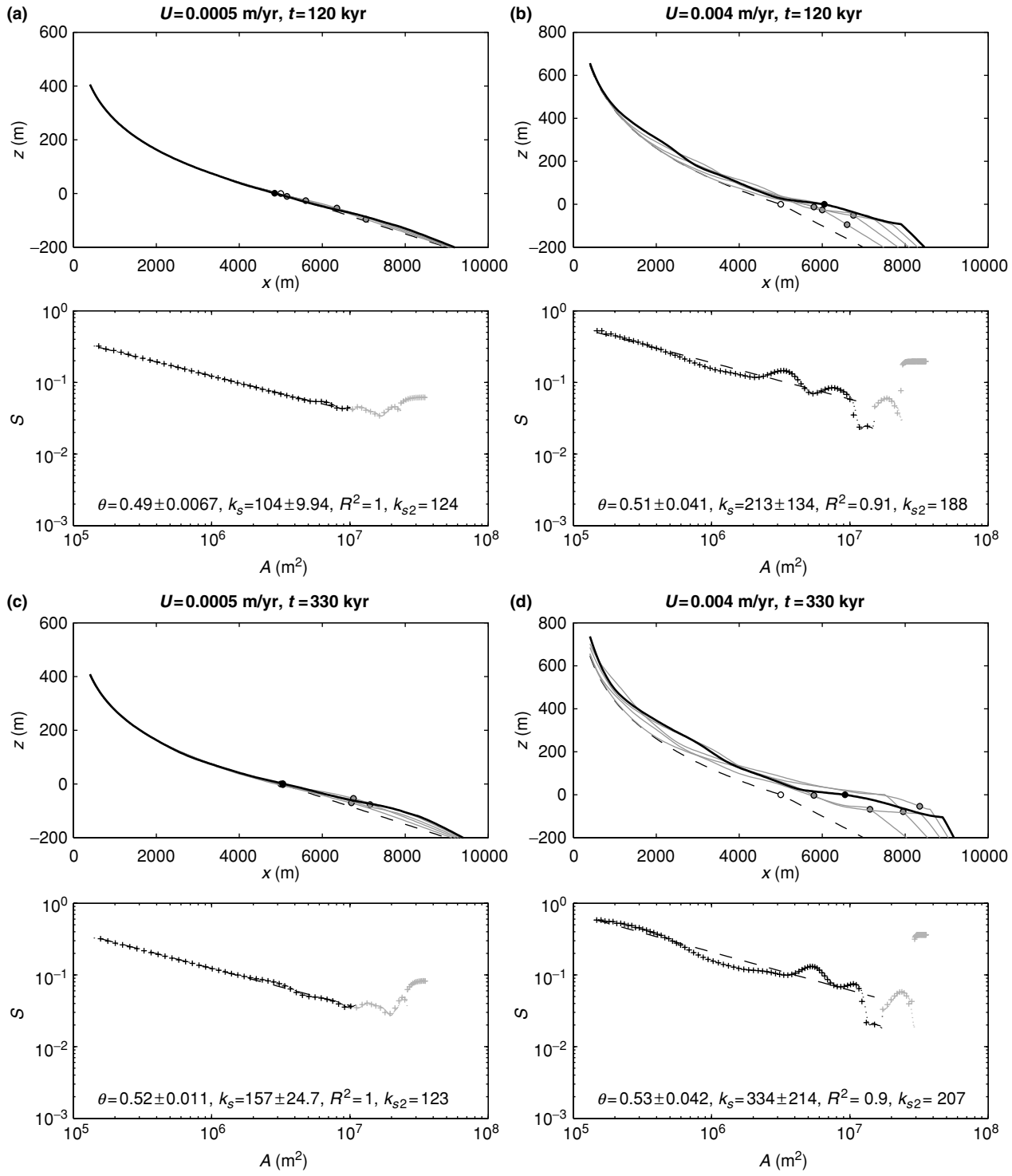

Fig. 10. Model results with Quaternary sea-level curve, and rapid drop in rock-uplift rate between $x = 5$ km and $x = 10$ km (uplift gradient boundary condition). See Figs 4 and 9 for description. (a) Single glacial–interglacial cycle (120 kyr), low-uplift rate. (b) Single glacial–interglacial cycle (120 kyr), high-uplift rate. (c) Multiple cycles (330 kyr), low-uplift rate. (d) Multiple cycles (330 kyr), high-uplift rate.

reaches a point where wave-base erosion balances uplift rates during regressions (Fig. 10). Slope–area regressions of data from quasi-steady-state channels with fixed x_{sl} by an offshore decrease in U should yield reasonable matches to theoretical parameters, provided that the channels have had sufficient time to equilibrate fully.

The integrated history of sea-level fluctuations introduces significant, systematic scatter to the S data (Fig. 10). The knickpoints and flats become less pronounced as they migrate upstream. This attenuation of eustatic effects is probably partially a real feature of slope variations in detachment-limited channels, as is the case for the

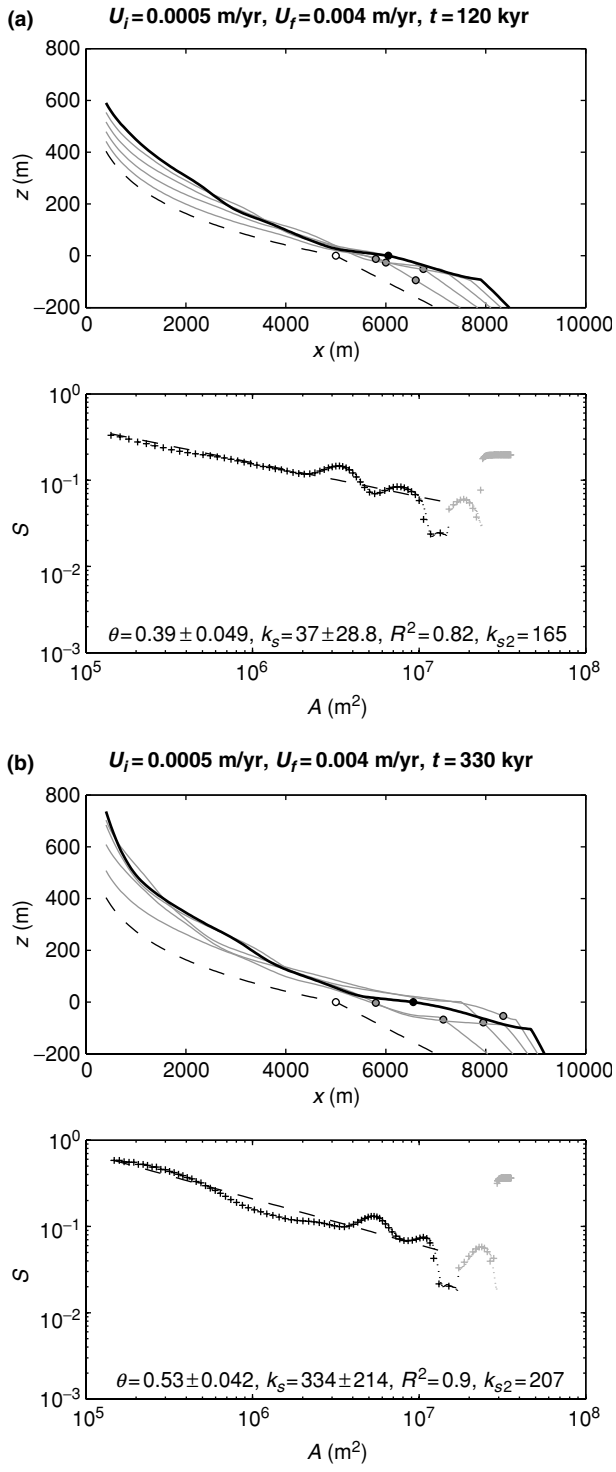

Fig. 11. Model results with Quaternary sea-level curve, transition from low- to high-uplift rate conditions, and uplift gradient boundary condition. See Figs 4 and 9 for description. (a) Single glacial–interglacial cycle (120 kyr). (b) Multiple cycles (330 kyr).

response of transport-limited channels (Schumm, 1993; Whipple & Tucker, 2002). However, part of this attenuation is undoubtedly the result of numerical diffusion because of the coarse model node spacing (50 m), as discussed by Baldwin *et al*. (2002). Slope datasets from real channels also exhibit scatter, particularly when derived from coarse (pixel size $\geq$ 10 m) digital elevation models (e.g. Snyder *et al*., 2000) (see also Fig. 13, below). Inaccuracies in data collection aside, gradients in steep, bedrock streams vary locally over ~50 m reaches because of variations in lithologic resistance, input of colluvium from adjacent hillslopes and many other factors (Snyder *et al*., 2000). These sorts of disruptions introduce nonsystematic scatter into S data, unlike the regular variations of Fig. 10. However, the modelling presented here suggests that some amount of the scatter seen in local channel gradients of coastal bedrock channels may be a result of fluctuating base level, particularly if these fluctuations were of higher frequency than those depicted in Fig. 8.

We have seen that short (5 km) channels adjust from the initial, artificial condition to a new quasi-steady-state form in just three eustatic cycles, given a steep drop off in uplift rates offshore. Now we consider the response to an acceleration in uplift rate. How can channels be expected to behave as they pass from low- to high-uplift conditions? The simulations presented in Fig. 11 illustrate such an acceleration. The initial condition is a 5 km channel adjusted to a low-uplift rate ($U = 0.0005$ m year^{-1}), with a steep offshore ramp (implicitly with an offshore decrease in uplift rate). The model runs with $U = 0.004$ m year^{-1} and the uplift-rate gradient boundary condition. In order to keep pace with high-uplift rates, the channel steepens from the mouth up. In 120 kyr, this wave of steepening has reached about half way up the length of the channel, and the shoreline position has regressed about 1 km (Fig. 11a). By 330 kyr, the channel has steepened to the divide, indicating nearly complete response (Fig. 11b). During the extra 210 kyr of the longer model run, the shoreline transgressed only another ~0.5 km. Given even more time, the shoreline position remains nearly static. Of course, longer channels would take longer to respond to uplift-rate changes (Whipple & Tucker, 1999).

Comparison to the Mendocino triple junction channels

We have studied extensively a set of 21 small, coastal streams near the Mendocino triple junction in northern California (Fig. 12; Snyder *et al*., 2000; Snyder, 2001; Snyder *et al*., 2002a,b). Rock-uplift rates vary along a 120 km long coast-parallel transect from 0.0005 m year^{-1} in the south to 0.004 m year^{-1} in the north (Merritts & Bull, 1989). In our previous studies, we have compared channel characteristics (gradient, lithology, width, discharge) from streams in the low-uplift zone to streams in the high-uplift zone (Fig. 13). In our initial analysis of watershed-scale topography from digital elevation models, we found that all the stream profiles were smooth and concave up, suggesting that they may be approximately in a steady state with uplift rates (Snyder *et al*., 2000). Our analysis of S–A data from the streams depended on the steady-state hypothesis, with the assumption that eustatic sea-level changes did not significantly affect the channel form. One of the goals of the modelling exercise presented

© 2002 Blackwell Science Ltd,

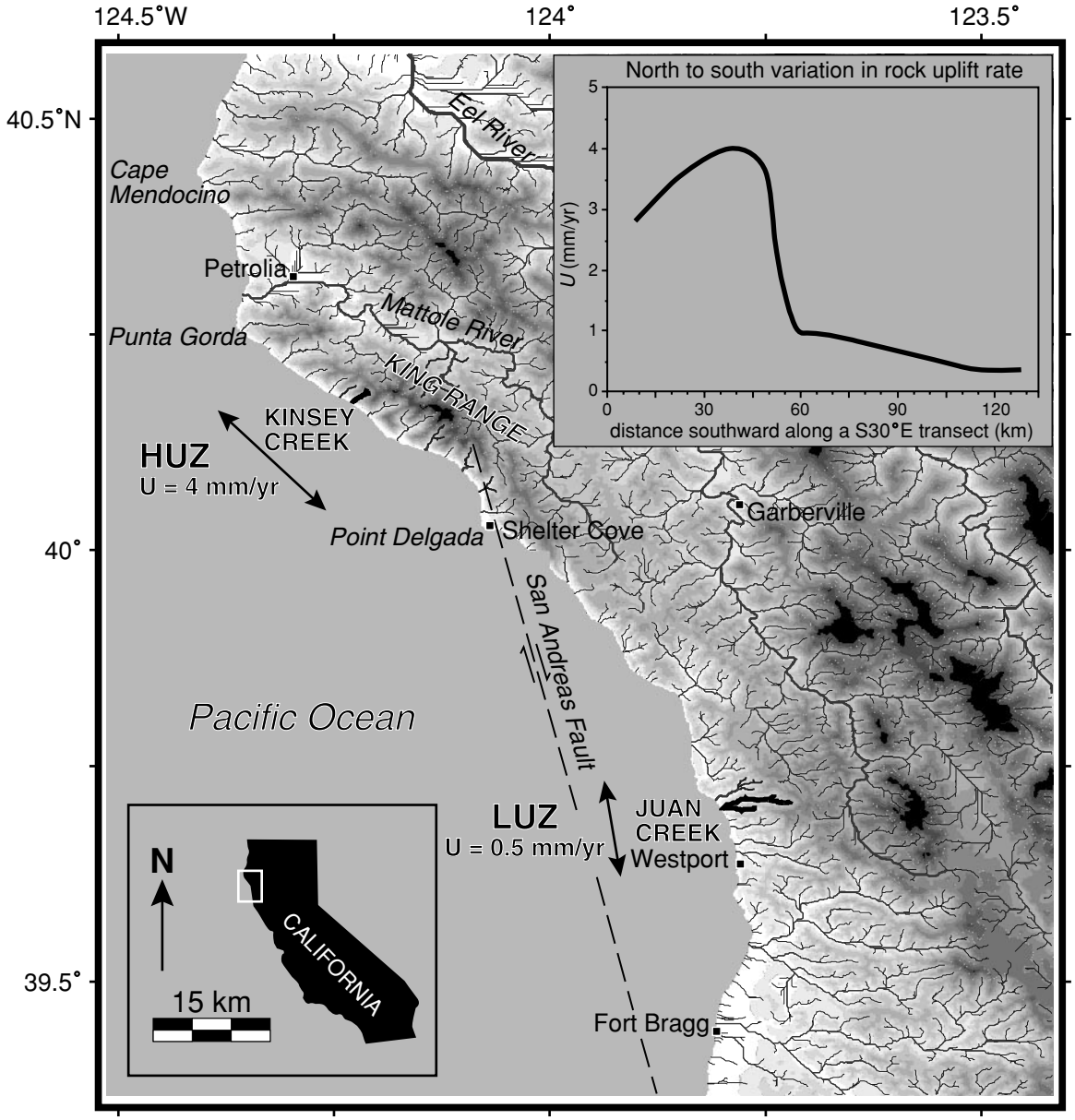

Fig. 12. Map of the Mendocino triple junction region of northern California, including the drainage network and elevation shading. Inset uplift-rate curve shows Late Pleistocene rock-uplift rates along a coast-parallel transect from Cape Mendocino to Westport, from a study of marine terraces by Merritts & Bull (1989). The two streams shown in Fig. 13 are marked, as are the high-uplift and low-uplift zones (HUZ and LUZ). Elevation shading ranges from white for 0–100 m to black for all areas over 1000 m.

here is to find the range of conditions where this assumption may be valid. A further goal is to compare the channel morphology predicted by the model to present-day channels.

As shown above, the steady-state hypothesis is compatible with channels experiencing complex base-level forcing if there is an offshore decrease in rock-uplift rates. At some distance offshore in the Mendocino triple junction region uplift rates must decrease, but little is known about the offshore tectonics. Because the uplift-rate data come from studies of emergent marine terraces, we have no information about how far the shoreline uplift rates extend into the Pacific Ocean. Therefore, we can only conclude that the steady-state hypothesis is consistent with an offshore decrease in rock-uplift rates in the Mendocino triple junction region. However, the analysis does suggest that the position of the shoreline in a tectonically active coast may be set by the location of a strong decline in uplift rate.

A surprising finding of longitudinal profile analyses of the California streams (Merritts & Vincent, 1989; Snyder *et al.*, 2000) was that the high-uplift rate channels have steepened (and therefore responded; Fig. 13) during the short, 100 kyr period since the onset of high-uplift rates (Merritts & Bull, 1989). As discussed by Whipple & Tucker (1999), response time is set by the change in elevation (or relief) necessary for the channel to adjust to the new conditions divided by the rate of elevation change (U–ε_f). For a given channel, this time will depend on a

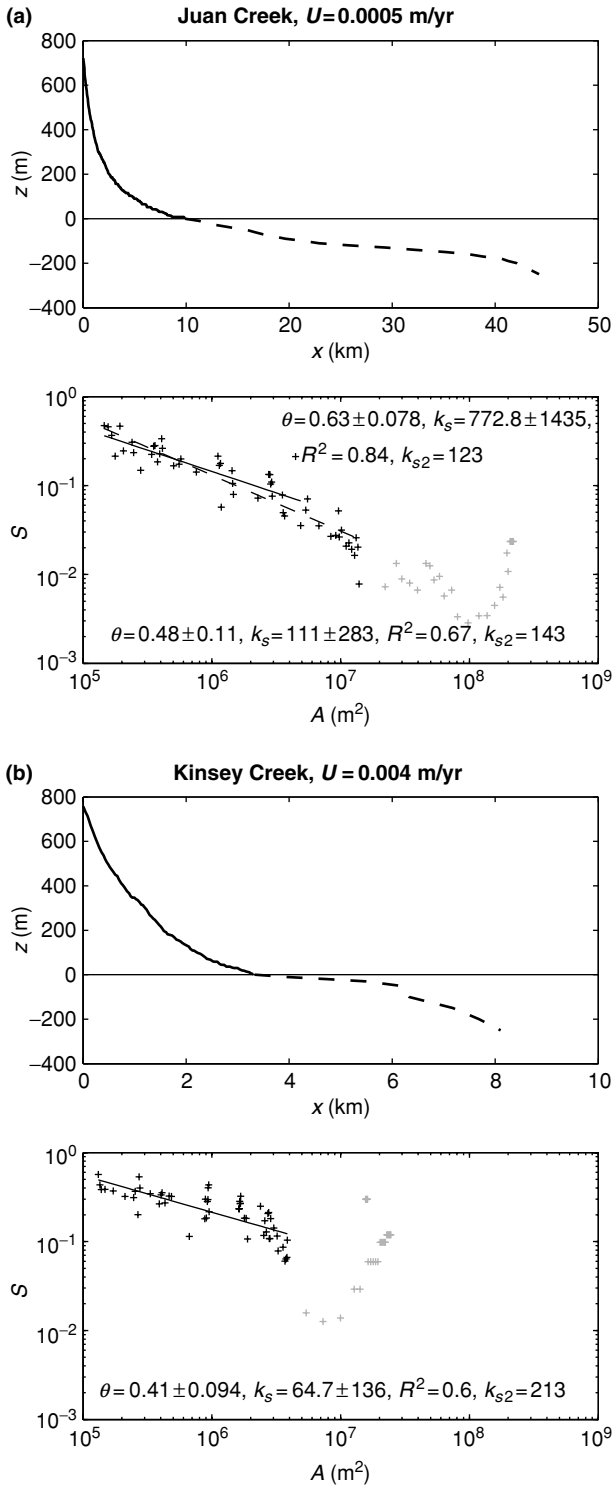

Fig. 13. Longitudinal-profile data for two streams in the Mendocino triple junction study area. Top panels are longitudinal profiles. Thick, solid line is the onshore fluvial channel, derived from USGS 30 m digital elevation models. Dashed line is the offshore bathymetry, extending perpendicular to contours from the channel mouth, digitized from 1 : 250 000 topographic – bathymetric maps. Bottom panels are plots of channel gradient (S) against drainage area (A). Dark crosses are onshore data points, gray crosses are offshore. Slopes are calculated on 10 m contour intervals, as done in our previous analysis of these streams (Snyder *et al.*, 2000). Regression lines are least-squares best fits to subsets of the onshore data, beginning at the top of the fluvial system ($A = 10^5$ m^2). Slight discrepancies between the regression fits on these plots and those in Snyder *et al.* (2000) reflect different regression domains. See Snyder *et al.* (2000) for full details on regression methodology. Thickness of channel-mouth alluvial deposits is unknown, but they are certainly thin compared to the longitudinal profile relief. (a) Juan Creek (low-uplift zone). Solid regression line is for the subset of data chosen to exclude the alluvial section at the mouth ($A < 5 \times 10^6$ m^2); best-fit parameters are shown in the lower left. Dashed regression line is the entire subset of onshore data; parameters are in upper right. (b) Kinsey Creek (high-uplift zone). Regression line is for the entire onshore channel.

variety of factors including channel length, rock-uplift rate and the fluvial erosion model parameters (Eqn. (1)). A theoretical calculation of response time, based on an assumed fixed base level, found that the channels should reach a new steady state in 50–200 kyr (Snyder *et al.*, 2000). The case modelled in Fig. 11 is essentially the situation for the high-uplift zone channels, with full response of a 5 km channel in about 330 kyr. Because the modelled scenario is highly simplified, this difference in response time is easily within uncertainty. The case simply shows that with a reasonable uplift-rate boundary condition, we might expect that the channels are in an approximate steady state, and therefore S–A regressions do yield reasonable estimates of Eqn. (1) model parameters.

The northern California streams typically exhibit a drop in gradient near their mouths (Fig. 13). This is particularly true in the case of larger streams and rivers (drainage area ≥ 10 km^2) of the region that have significant alluvial deposits at their mouths (Merritts *et al.*, 1994; Snyder *et al.*, 2000). For this reason we limited our profile analysis to drainage areas less than 5 km^2—a value conservatively chosen in order to avoid process transitions from erosive bedrock channels to depositional alluvial channels (Snyder *et al.*, 2000). Smaller channels, such as Kinsey Creek, also have a package of alluvium at the mouth, though any slight reduction in slope does not extend far enough upstream to affect the S–A analysis significantly (Fig. 13b). As discussed by Merritts *et al.* (1994), alluviation of uplifting river mouths is expected during the post-transgression stillstand (last 6 kyr), when offshore wave-cut platforms begin to emerge as channel mouths. We see this situation in the model runs, particularly for the high-uplift cases, where U is significantly greater than that of the latest Holocene rate of sea-level rise. This is also the case in $U = 0.0005$ m year^{-1} model runs when S_{ramp} is less than 0.05. Of course, the model is not tracking sediment deposition, and the large drop in slope of the high-uplift channel mouths (i.e. Fig. 10b and d) would undoubtedly be attenuated by sediment deposition in a more sophisticated fluvial model.

As discussed and modelled elsewhere (e.g. Bloom *et al.*, 1974; Merritts & Bull, 1989; Cinque *et al.*, 1995; Anderson *et al.*, 1999), uplifting coastlines are commonly identified by emergent marine terraces, as is the case in the Mendo-

© 2002 Blackwell Science Ltd,

cino triple junction region. The only point we would like to add about marine terraces relates to the uplift-rate boundary condition. The narrow (< 100 m, Merritts *et al.*, 1992), young (< 100 kyr, since an acceleration in uplift rates, Merritts & Bull, 1989), emergent marine terraces around Cape Mendocino, abandoned after minor Late Pleistocene highstands (Fig. 8), are consistent with the modest shoreline advance predicted with a steep uplift-rate gradient (i.e. Fig. 11). If high-uplift rates extend very far offshore, then we might expect to see a wider zone of newly emergent (post-100 ka) marine terraces as the shoreline transgresses rapidly (i.e. Fig. 9b and d). Much of the northern California coast (including the older, higher terraces of the Cape Mendocino area) exhibits a flight of wide (~1 km) marine terraces (e.g. Merritts *et al.*, 1992; Anderson *et al.*, 1999), which may be consistent with only minor offshore gradients in uplift rates. The modelling presented here suggests that the development and evolution of marine-terraced coastlines should depend critically on the offshore uplift-rate conditions.

The bathymetry of the Mendocino triple junction area shares some similarities with the model bathymetry. In the high-uplift zone, the nearshore (3–5 km) seabed gradient is quite low ($S \approx 0.02$), whereas farther offshore the gradient is much steeper ($S \approx 0.1$; Fig. 13b). Of course, the models reflect this, with flat wave-cut platforms in the nearshore and steeper conditions offshore (set by S_{ramp}). However, the seabed offshore from Juan Creek has a fairly constant gradient around 0.01 (Fig. 13a)—a situation not represented particularly well by the model profiles. This real difference in shelf morphology may reflect differing tectonic settings or differing wave climates. Moreover, the shelf of the northern California coast is cut in many places by large canyons (similar to those discussed by Talling, 1998), which are also totally ignored by the model. Further advances in our ability to model channel response to eustatic fluctuations will depend on the development of more sophisticated wave-base bedrock erosion models.

CONCLUSIONS: CHANNEL RESPONSE TO EUSTATIC FORCINGS

Our modelling efforts show that the response of uplifting bedrock streams to fluctuations in base level caused by eustasy depends fundamentally on three factors: (i) nearshore bathymetry, (ii) the relationship between the relative rate of base-level change and wave-base erosion and (iii) offshore rock-uplift conditions. Here we review some of our findings and suggest avenues for further field research and modelling.

The details of channel response to any given regression are set by the nearshore bathymetry. The development of bathymetry depends on eustatic sea-level changes, rock-uplift rate and wave-base erosion. The model presented here treats the latter in the simplest possible manner, ignoring many important controls on the evolution of shelf morphology, including wave dissipation as a function of width, stochastic influences on wave energy and direction, sediment deposition and erosion of offshore canyons. Further advances in the modelling of channel response to fluctuating sea level will depend on development of a proper wave-base bedrock erosion law. Though much is known about sediment transport in coastal environments, relatively little has been done on erosion of bedrock. Measurements by Adams *et al.* (2000) of delivery of wave energy to coastlines represent an exciting new research direction to achieve the goal of understanding the evolution of shelf bathymetry on uplifting coastlines.

Channels lengthen over time when rock-uplift rates exceed wave-base erosion rates. This simple fact is not generally included in river-incision modelling efforts, which treat the case of block uplift relative to a fixed base level. However, the model presented here shows that channel lengthening changes the response to uplift quite remarkably. If onshore rock-uplift rates extend far into the offshore, then channels will generally grow seaward. Along with the increase in length comes an increase in divide-to-mouth relief, and changes in stream-profile concavity and steepness. The regression persists until the shoreline reaches a zone where rock-uplift rates decrease. A stable maximum regression shoreline position is attained at the point where the relative rate of base-level fall (uplift rate plus regressing sea level) balances wave-base erosion. Once the channel reaches this position, it ceases to lengthen significantly, and relief ceases to increase. Only then the channel can evolve toward an approximate steady-state condition, with fluvial incision rates balancing uplift rates. This condition will persist until a key forcing changes, such as tectonic regime, climate, or magnitude of sea-level oscillations. The offshore uplift-rate conditions are the most important control on the overall development of drainage basins and fluvial relief when eustatic forcing is considered.

ACKNOWLEDGEMENTS

This paper benefited from discussions and correspondence with Robert Anderson, Neal Driscoll, Bill Lyons and Matt Reuer and reviews by Anderson, Kip Hodges, Frank Pazzaglia and John Southard.

REFERENCES

Adams, P.N., Anderson, R.S. & Revenaugh, J.S. (2000) Seismic measurements of the shaking of seacliffs: determining the relative effects of oceanographic variables. *EOS, Transactions, AGU*, **81,** F508.

Anderson, R.S., Densmore, A.L. & Ellis, M.A. (1999) The generation and degradation of marine terraces. *Basin Res.*, **11,** 7–19.

Antoine, P., Lautridou, J.P. & Laurent, M. (2000) Long-term fluvial archives in NW France: response of the Seine and Somme rivers to tectonic movements, climatic variations and sea-level changes. *Geomorphology*, **33,** 183–207.

Baldwin, J.A., Whipple, K.X. & Tucker, G.E. (2002) Implications of the shear-stress river incision model for the post-orogenic decay of topography. *J. Geophys Res.*, **107,** in press.

Bloom, A.L., Broecker, W.W., Chappell, J.M.A., Mathews, R.K. & Mesolella, K.J. (1974) Quaternary sea-level fluctuations on a tectonic coast: New $^{230}Th/^{234}U$ dates from the Huon Peninsula, New Guinea. *Quaternary Res.*, **4,** 185–205.

Chappell, J. (1974) The geomorphology and evolution of small valleys in dated coral reef terraces, New Guinea. *J. Geol.*, **82,** 795–812.

Chappell, J., Omura, A., Esat, T., McCulloch, M., Pandolfi, J., Ota, Y. & Pillans, B. (1996) Reconciliation of late Quaternary sea levels derived from coral terraces at Huon Peninsula with deep sea oxygen isotope records. *Earth Planetary Sci. Lett.*, **14,** 227–236.

Christie-Blick, N. & Driscoll, N.W. (1995) Sequence stratigraphy. *Annu. Rev. Earth Planetary Science*, **23,** 451–478.

Cinque, A., De Pippo, T. & Pomano, P. (1995) Coastal slope terracing and relative sea-level changes: deductions based on computer simulations. *Earth Surface Processes and Landforms*, **20,** 87–103.

Hack, J.T. (1973) Stream profile analysis and stream-gradient index. *J. Res. U.S. Geol. Survey*, **1,** 421–429.

Howard, A.D. & Kerby, G. (1983) Channel changes in badlands. *Geol. Soc. Am. Bull.*, **94,** 739–752.

Howard, A.D., Seidl, M.A. & Dietrich, W.E. (1994) Modeling fluvial erosion on regional to continental scales. *J. Geophys Res.*, **99,** 13,971–13,986.

Imbrie, J., Hays, J.D., Martinson, D.G., McIntyre, A., Mix, A.C., Morley, J.J., Pisias, N.G., Prell, W.L., Shackleton, N.J. (1984) The orbital theory of Pleistocene climate: support from a revised chronology of the marine $\delta^{18}0$ record. In: *Milankovitch and Climate* (Ed. by A.L. Berger, J. Imbrie, J. Hays, G. Kukla & B. Saltzman), pp. 269–305. D. Reidel, Dordrecht, The Netherlands.

Kirby, E. & Whipple, K.X. (2001) Quantifying differential rock-uplift rates via stream profile analysis. *Geology*, **29,** 415–418.

Merritts, D. & Bull, W.B. (1989) Interpreting Quaternary uplift rates at the Mendocino triple junction, northern California, from uplifted marine terraces. *Geology*, **17,** 1020–1024.

Merritts, D.J., Chadwick, O.A., Hendricks, D.M., Brimhall, G.H. & Lewis, C.J. (1992) The mass balance of soil evolution on late Quaternary marine terraces, northern California. *GSA Bull.*, **104,** 1456–1470.

Merritts, D. & Vincent, K.R. (1989) Geomorphic response of coastal streams to low, intermediate, and high rates of uplift, Mendocino junction region, northern California. *Geol. Soc. Am. Bull.*, **101,** 1373–1388.

Merritts, D.J., Vincent, K.R. & Wohl, E.E. (1994) Long river profiles, tectonism, and eustasy: a guide to interpreting fluvial terraces. *J. Geophys Res.*, **99,** 14031–14050.

Middleton, G.V. (1973) Johannes Walther's law of correlation of facies. *Geol. Soc. Am. Bull.*, **84,** 979–988.

Pazzaglia, F.J., Gardner, T.W. & Merritts, D.J. (1998) Bedrock fluvial incision and longitudinal profile development over geologic timescales determined by fluvial terraces. In: *Rivers Over Rock: Fluvial Processes in Bedrock Channels* (Ed. by K.J. Tinkler & E.E. Wohl), pp. 207–236. American Geophysical Union, Washington, USA.

Pitman, W.C. (1978) Relationship between eustacy and stratigraphic sequences of passive margins. *Geol. Soc. Am. Bull.*, **89,** 1389–1403.

Schumm, S.A. (1993) River response to base-level change: implications for sequence stratigraphy. *J. Geol.*, **101,** 279–294.

Sklar, L. & Dietrich, W.E. (1998) River longitudinal profiles and bedrock incision models: stream power and the influence of sediment supply. In: *Rivers Over Rock: Fluvial Processes in Bedrock Channels* (Ed. by K.J. Tinkler & E. E Wohl), pp. 237–260. American Geophysical Union, Washington, DC., USA.

Snyder, N.P. (2001) *Bedrock Channel Response to Tectonic, Climatic and Eustatic Forcings*. PhD Thesis, Deptartment of Earth, Atmospheric, and Planetary Sciences, Massachusetts Institute of Technology, Cambridge, UK.

Snyder, N.P., Whipple, K.X., Tucker, G.E. & Merritts, D.J. (2000) Landscape response to tectonic forcing: DEM analysis of stream profiles in the Mendocino triple junction region, northern California. *Geol. Soc. Am. Bull.*, **112,** 1250–1263.

Snyder, N.P., Whipple, K.X., Tucker, G.E. & Merritts, D.J. (2002a) Channel response to tectonic forcing: analysis of stream morphology and hydrology in the Mendocino triple junction region, northern California. *Geomorphology*, in press.

Snyder, N.P., Whipple, K.X., Tucker, G.E. & Merritts, D.J. (2002b) The importance of a stochastic distribution of floods and erosion thresholds in the bedrock river incision problem. *J. Geophys. Res.*, in review.

Stock, J.D. & Montgomery, D.R. (1999) Geologic constraints on bedrock river incision using the stream power law. *J. Geophys. Res.*, **104,** 4983–4993.

Summerfield, M.A. (1985) Plate tectonics and landscape development on the African continent. In: *Tectonic Geomorphology* (Ed. by M. Morisawa & J.T. Hack), pp. 27–51. Allen & Unwin, Boston.

Summerfield, M.A. (1991) *Global Geomorphology*. Longman Group Ltd, Harlow, England.

Sunamura, T. (1992) *Geomorphology of Rocky Coasts*. John Wiley & Sons, New York, USA.

Talling, P.J. (1998) How and where do incised valleys form if sea level remains above the shelf edge? *Geology*, **26,** 87–90.

Tebbens, L.A., Veldkamp, A. & Van Dijke, J.J. (2000) Modeling longitudinal-profile development in response to Late Quaternary tectonics, climate and sea-level changes: the River Meuse. *Global Planetary Change*, **27,** 165–186.

Tucker, G.E., Lancaster, S.T., Gasparini, N.M. & Bras, R.L. (2001) The channel-hillslope integrated landscape development (CHILD) model. In: *Landscape Erosion and Evolution Modeling* (Ed. by R.S. Harmon & W. W. Doe), pp. 349–388. Kluwer Academic/Plenum Publishers, New York, USA.

Tucker, G.E. & Whipple, K.X. (2002) Topographic outcomes predicted by stream erosion models: sensitivity analysis and intermodel comparison. *J. Geophys. Res.*, **107,** in press.

Vail, P.R., Mitchum, R.M., Todd, R.G., Widmier, J.M., Thompson, S., Sangree, J.B., Bubb, J.N. & Hatlelid, W.G. (1977) Seismic stratigraphy and global changes of sea level. In: *Seismic Stratigraphy-Applications to Hydrocarbon Exploration* (Ed. by C.E. Payton), pp. 49–212. The American Association of Petroleum Geologists, Tulsa, Oklahoma, USA.

Veldkamp, A. & Van Dijke, J.J. (1998) Modelling long-term erosion and sedimentation processes in fluvial systems: a case study for the Allier/Loire system. In: *Paleohydrology and Environmental Change* (Ed. by G. Benito & V.R. Baker & K. J. Gregory), pp. 53–66. John Wiley and Sons, New York, USA.

Veldkamp, A. & Van Dijke, J.J. (2000) Simulating internal and external controls on fluvial terrace stratigraphy: a qualitative comparison with the Maas record. *Geomorphology*, **33,** 225–236.

Wheeler, H.E. (1964) Baselevel, lithosphere surface, and time-stratigraphy. *Geol. Soc. Am. Bull.*, **75,** 599–610.

© 2002 Blackwell Science Ltd,

Whipple, K.X., Anderson, R.S. & Hancock, G.S. (2000) River incision into bedrock: mechanics and relative efficacy of plucking, abrasion, and cavitation. *Geol. Soc. Am. Bull.*, **112,** 490–503.

Whipple, K.X. & Tucker, G.E. (1999) Dynamics of the stream-power river incision model: implications for the height limits of mountain ranges, landscape response timescales, and research needs. *J. Geophys. Res.*, **104,** 17661–17674.

Whipple, K.X. & Tucker, G.E. (2002) Implications of sediment-flux-dependent river incision models for landscape evolution. *J. Geophys. Res.*, **107,** in press.

Willet, S.D., Slingerland, R. & Hovius, N. (2001) Uplift, shortening, and steady state topography in active mountain belts. *Am. J. Sci.*, **301,** 455–485.

Willgoose, G., Bras, R.L. & Rodriguez-Iturbe, I. (1991) A coupled channel network growth and hillslope evolution model,1 theory. *Water Resources Res.*, **27,** 1671–1684.

Manuscript accepted 8 March 2002